

**FRET-BASED BIOSENSORS TO ELUCIDATE EXTRACELLULAR SIGNAL-  
REGULATED KINASE (ERK) DYNAMICS**

By  
Archer R. Hamidzadeh

A thesis submitted to Johns Hopkins University in conformity with the requirements for  
the degree of Master of Science in Engineering

Baltimore, MD  
May, 2015

## **Abstract**

Proper cell functions are dependent on the precise regulation of transduction events to relay external environmental cues into the cell for processing. The propagation and regulation of the signal involves a diverse array of enzymes and molecules with distinct functions and differences in spatio-temporal regulation. Further understanding cell signaling dynamics will continue to provide a knowledge basis for developing disease therapies. While an active field of research, a great deal of information has remained elusive with the previously used tools to monitor such pathways either through discrete snapshots or analyses of single components of signaling pathways outside of their natural biological context. To address these limitations, FRET-based biosensors provide a powerful means to dissect the complexities of signaling pathways in a real-time manner in live cells.

The first objective is to optimize the previously developed ERK Activity Reporter, EKAR, by examining the dependence of its dynamic range on fluorophore orientation. To alter relative fluorophore orientations, variations of EKAR were developed with reversed orders of fluorescent proteins. Reversing the order of a previously optimized yellow-cyan EKAR led to a cyan-yellow EKAR with an improved dynamic range. Moreover, a closer examination of the previously optimized EeVee-linker, which was believed to render FRET-based biosensors solely distance-dependent, reveals that the FRET efficiency is likely dependent on FP orientation in EeVee-linker based biosensors. This conclusion for EKAR can likely be extended for further improvements of other FRET-based biosensors with the EeVee linker.

The second objective is to expand the versatility of the EKAR biosensor for co-imaging capabilities, which allow for more precise correlations between multiple activity readouts on a single-cell level. Utilizing EKAR color variants, a co-imaging strategy was employed to allow for imaging two sensors with spectrally distinct FRET-donor fluorescent proteins (FP) and a common FRET-acceptor FP. This strategy allowed for simultaneously tracking ERK activity in multiple subcellular compartments, monitoring both ERK and Protein kinase A (PKA) on a single-cell level, and for the development of a novel single-chain biosensor capable of monitoring ERK and Ras activity in the plasma membrane.

Continued investigations will provide powerful tools to elucidate signaling dynamics with stronger precision.

**Thesis advisors and readers:**

Professors Jin Zhang, Andre Levchenko, and Kevin Yarema

## Preface

Foremost, I would like to express my immense gratitude to my advisors, Professor Jin Zhang and Professor Andre Levchenko, for their incredible guidance and support during my undergraduate and graduate studies. I greatly appreciate their motivation, enthusiasm, and vast knowledge in the area of cellular signaling, all of which have allowed me to grow towards becoming an independent researcher. I owe my great enthusiasm to continue studying biological signaling to both of them. In addition, I would like to express my immense gratitude to Professor Kevin Yarema for his invaluable comments and guidance for this thesis.

In addition, I would like to thank the other members of both labs, who have provided excellent environments to conduct these research projects, collaborate, and learn. I greatly appreciate the guidance and mentoring from everyone in these two labs. A great deal of appreciation is due to my research mentor, and good friend, Dr. Ambhi Ganesan. He has truly been an excellent guide and friend throughout my studies.

I would also like to thank my earliest research and academic advisers at Hopkins, Dr. Vincent Hilser and Dr. Ludwig Brand, who guided me towards the right path - quantitatively understanding biological phenomena.

Last but not least, I am indebted to my father, Dr. Hamid Hamidzadeh, my mother, Azar, and my brother, Cyrus, for their unconditional compassion and support over the years.

## Table of Contents

<b>Title Page</b> .....	i
<b>Abstract</b> .....	ii
<b>Preface</b> .....	iii
<b>Table of Contents</b> .....	iv
<b>List of Figures</b> .....	v
<b>Introduction</b> .....	1-15
<b>Chapter 1</b>	
Optimization of FRET-based Biosensor for Investigation of Extracellular Signal-Regulated Kinase Dynamics.....	16-33
ERK-MAPK signaling.....	17
Regulation of ERK activity and specificity.....	20
Optimization of EKAR.....	22
Methods.....	30
References.....	32
<b>Chapter 2</b>	
Expansion of the Application of EKAR for Investigation of Extracellular Signal Regulated Kinase Dynamics.....	34-54
Development and characterization of EKAR color variants.....	35
Visualization of ERK activity in the cytoplasm.....	42
ERK activity in the plasma membrane and nucleus.....	44
Co-Imaging of subcellular-targeted EKAR.....	48
Methods.....	51
References.....	53
<b>Chapter 3</b>	
Investigation of Crosstalk and Pathway dynamics of Extracellular Signal- Regulated Kinase.....	55-76
Biological crosstalk: cAMP-PKA and ERK-MAPK pathways.....	56
EKAR and AKAR co-imaging.....	57
Role of calcium in the ERK-MAPK pathway.....	65
Simultaneously monitoring the activities of Ras and ERK.....	66
Methods.....	74
References.....	76
<b>Curriculum Vitae</b> .....	77

## List of Figures

<b>Figure 1.1</b>	ERK-MAPK cascade.....	18
<b>Figure 1.2</b>	Average EGF-induced responses of cyan-yellow EKARs.....	24
<b>Figure 1.3</b>	Average dynamic ranges of cytoplasmic-targeted cyan-yellow EKARs....	25
<b>Figure 1.4</b>	Effects of EeVee linker length on EKAR dynamic range.....	27
<b>Figure 1.5</b>	Effects of EeVee linker length on EKAR basal FRET values.....	29
<b>Figure 2.1</b>	Design and characterization of diffusible EKAR color variants.....	38
<b>Figure 2.2</b>	Representative characterization experiments of EKAR color variants.....	39
<b>Figure 2.3</b>	Average dynamic ranges of diffusible EKAR color variants.....	41
<b>Figure 2.4</b>	Cytoplasmic targeting of EKAR.....	43
<b>Figure 2.5</b>	Plasma membrane and nuclear targeting of EKAR.....	46
<b>Figure 2.6</b>	Targeted EKAR Co-Imaging.....	50
<b>Figure 3.1</b>	EKAR and AKAR co-imaging.....	59
<b>Figure 3.2</b>	EKAR and AKAR co-imaging controls.....	62
<b>Figure 3.3</b>	EKAR control under co-imaging stimulus conditions.....	64
<b>Figure 3.4</b>	SABER1.0.....	68
<b>Figure 3.5</b>	SABER1.0: single cell results - Oscillatory Ras Response.....	70
<b>Figure 3.6</b>	SABER1.0: single cell results - Sustained Ras Response.....	71
<b>Figure 3.7</b>	SABER1.0: mutant control.....	72

Intended to be blank

# **Introduction**



## **Cellular Signaling**

With the realization that cells do not live in isolation, cellular communication is an inherent process that drives functional responses of a cell to its surrounding environment. This process of exchanging messages between a cell and its environment is present in all cells. Single-celled prokaryotes sense and navigate toward nutrients sources. Eukaryotic microorganisms, such as yeasts and protozoans, utilize secreted pheromones to coordinate aggregation and mating. Lastly, multicellular eukaryotes use a plethora of signaling molecules and mechanisms to coordinate the developmental, regulatory, and metabolic activities of the organism as a whole. Signal transduction cascades are molecular circuits responsible for sensing, amplifying, and integrating various external environmental stimuli into intracellular responses, such as changes in gene expression and enzyme activity. A signaling cascade is generally triggered by the binding of a ligand to a specific protein receptor. The subsequent conformational change results in the initiation of one or more pathways that transmit the stimulus to the interior of the cell. These cascades, which involve a complex network of interwoven molecules, enzymes, and transcription factors, control cellular responses such as: proliferation, differentiation, and apoptosis.

Normal cell function is dependent on the precise regulation of transduction events to relay the external environmental cue into an intracellular outcome. The propagation and regulation of the signal involves a diverse array of enzymes with distinct functions. In particular, post-translational modifications (PTMs) of cellular proteins are important mechanisms for propagating the signal. One of the more common PTMs, phosphorylation, has a governing role in many signaling events. Protein kinases

enzymatically transfer the  $\gamma$ -phosphate from adenosine triphosphate (ATP) to serine, threonine, or tyrosine residues of a target protein, resulting in changes in the protein's activity, localization, or interactions (1).

The human genome is reported to contain 518 protein kinase genes, about 2% of all known human genes (2). While protein kinases share a conserved catalytic core, various structural components dictate their activation, regulation, target protein preferences, and localization within the cell (3). These kinases modify several downstream targets, which comprise 30% of all human proteins. The dynamics of kinase levels, activities, and localization influence the regulation of major processes in the cell. Dysregulation of kinase function or localization is a hallmark of numerous diseases including neurodegenerative, autoimmune, and immunological disorders and most human cancers. Due to their roles in various cellular activities and pathologies, kinases have been prime targets for therapies. Over the past two decades, a small number of small-molecule kinase inhibitors have been identified and approved for clinical use (4).

Conventional methods of investigating kinase activity involve quantification of the phosphoryl transfer using enzyme-based and lysis-based radiometric or phospho-specific antibody assays *in vitro*. Traditional radioisotope filtration binding assays utilize radioisotope labeled  $\gamma$ -ATP reactions and cumbersome binding and washing steps for the ultimate detection of kinase activity (5). Moreover, later assays were directed to detect kinase activity using phospho-specific antibodies or fluorescent signals (6). While these methods have been successful in detecting kinase activity and function, a great deal of information is lost when monitoring the activity of these enzymes outside of the cell or in discrete snapshots through Western blots and immunostaining. Further understanding

the strict spatiotemporal regulation of kinases in the context of their intact, instructive biological network would provide greater insight into the complex system that is cellular signaling and for the rational design of therapeutic agents for these enzymes.

The challenges posed by previous methods for investigating enzyme activity in a non-destructive and real-time manner have been addressed by rapidly flourishing and novel fluorescence technology (7, 8). Genetically encoded fluorescence resonance energy transfer (FRET)-based biosensors have been applied both in vivo and in vitro to analyze both the temporal dynamics and subcellular compartmentalization within signaling events.

### **The emergence of FRET-based biosensors**

Over 70 years ago, Theodor Förster published his now influential paper on the theory of electronic energy transfer (9). An excited fluorophore can return to its ground state by emitting photons, non-radiative dissipation, transitioning to a non-fluorescent triplet state, or by transferring energy to an aptly oriented dipole of an adjacent fluorophore. Förster, or fluorescence, resonance energy transfer (FRET) is the process of radiationless transport of energy from a donor to acceptor fluorophore in the range of 1-10 nanometers (9-11). FRET efficiency (E) is governed by the interfluorophore distance (r) and Förster radius (r<sub>0</sub>), the distance at which energy transfer efficiency is 50%. FRET efficiency is given by the formula: 
$$E = \frac{1}{1 + \left(\frac{r}{r_0}\right)^6} .$$

The Förster radius is a function of the spectral overlap of the donor emission and acceptor excitation spectra (J), the orientation of the dipoles (k<sup>2</sup>), the refractive index of the media (n), and the quantum yield of the donor (Q<sub>0</sub>) in the absence of the acceptor

fluorophore (8, 12). The Förster radius is calculated by  $r_0^6 = \frac{9000 Q_0 (\ln 10) J k^2}{128 \pi^5 n^4 N_A}$ , where  $N_A$  is Avogadro's number.

Since the discovery of green fluorescent protein (GFP) in the early 1960s, efforts to improve fluorescent protein (FP) technology have produced a considerable number of engineered FP variants and have resulted in the expansion of the color palette into blue, cyan, red, and orange spectra (13-15). Moreover, during the past two decades, significant improvements have been made in FP folding (16, 17), photostability (18), maturation (19), and brightness (20, 21) for use in mammalian cell systems. Particular pairs of these FP variants can undergo FRET at high efficiencies. The increasing availability of FPs with diverse physical properties and parameters aids scientific research in various experimental situations.

In the context of the biophysical investigation of cellular signaling, FRET-based biosensors have been designed to bring a fluorophore pair in close proximity for FRET in a variety of ways and for visualization of diverse cellular events. For example, two FRET fluorophores can be situated close together and flanking a protease cleave site on a protein to continuously undergo FRET until disrupted by a specific cellular protease (22, 23). Alternatively for kinase sensors, a kinase-specific substrate domain linked to a phosphopeptide-binding domain can be flanked by a FRET pair (24, 25). Upon phosphorylation, the binding of the two domains brings the two fluorophores spatially close and thus, increasing FRET.

FRET-based biosensor strategies commonly rely on such conformational changes in the biosensor induced by recognition or post-translational modification events of a protein of interest. Based on the ratio of the FRET/donor emission signals and changes in

the duration of the fluorophore remaining in an excited state, the dynamics in concentration or activity of a specific signaling component can be determined (26). Live cell imaging with these FRET-based biosensors has allowed deeper investigation of cellular signaling regulation (27-28).

### **Rational design of FRET-based kinase activity reporters**

Among the numerous biosensors used for analyzing the subcellular dynamics of molecules and proteins, kinase activity reporters constitute an important subset for a deeper understanding of the dynamics of one of the main post-translational modifications, phosphorylation. These biosensors act as surrogate substrates and a variety of such have been developed for a number of serine/threonine and tyrosine kinases, such as extracellular signal-regulated kinases (ERK) (29, 30), cAMP-dependent protein kinase (PKA) (31, 32), c-Jun N-terminal kinases (33), and Src kinases (34, 35). These kinase reporters utilize a general modular design (7) composed of a molecular switch dependent on kinase activity flanked by a pair of fluorescent proteins able to undergo FRET. The molecular switch consists of a substrate domain of the kinase of interest and a phosphoamino acid binding domain. Upon phosphorylation of the substrate domain and the subsequent binding of this phosphorylated domain by the phosphoamino acid binding domain, the distance and relative orientation of the flanking fluorescent proteins are changed and thus causing a change in FRET. The resulting changes in FRET can be monitored by fluorescence microscopy.

The modular design of such biosensors allows a general ease for researchers to develop specific reporters for a number of kinases by the careful selection of a substrate

domain for the kinase of interest and a phosphoamino acid binding domain. Moreover, the design allows for testing of various fluorophore pairs for sufficient quantitative detection and dynamic range of the biosensor. For investigations of a particular kinase, the biosensor requires a substrate domain that is not only specifically phosphorylated by the kinase of interest, but also efficiently phosphorylated by the kinase. The biosensor also requires a phosphoamino acid binding domain that can readily recognize the phosphorylated substrate, such that the phosphorylation event can easily be converted to an intramolecular conformational change caused by the binding of the two.

An optimized kinase biosensor must be specific, sensitive to detect small changes, and reversible. While a kinase activity reporter requires a selective substrate of the kinase, certain classes of kinases, notably the class of mitogen-activated protein kinases, recognize similar phosphorylation sites composed of a serine/threonine followed by a proline (36). Substrate specificity can be enhanced by adding a kinase specific docking site that allows for stronger interactions with the kinase and thus enhancing the efficiency of phosphorylation. Sensitivity to small changes in kinase activity is determined by the dynamic range of the reporter and can vary. Increased sensitivity can be achieved by designing reporters with greater differences in the FRET efficiencies between the unphosphorylated and phosphorylated states. As surrogate substrates, kinase activity reporters should be able sensitive to detect small changes in kinase activity as one active kinase can phosphorylate multiple reporters and thus amplify the response. Moreover, reversible reporters allow for continuous monitoring of kinase activity in the context of the intact biological network composed of the kinase and phosphatases. Reversibility can be enhanced by the use of phosphoamino acid domains with weaker binding affinity,

modifying the substrate sequence, or incorporating sequences for phosphatase recruitment (33).

Kinase activity reporters have a number of distinct advantages. Such biosensors are engineered as DNA constructs and expressed in living cells from a single gene. This approach avoids the significant problems of macromolecule delivery and allows for real-time and quantitative monitoring of kinase activity within the natural biological context with high temporal resolution. These biosensors can also be tagged with intracellular targeting sequences to investigate kinase activity in particular subcellular regions, such as the plasma membrane or nucleus, and thus allows for high spatial resolution. Moreover, the utilization of FRET allows for improved signal-to-noise ratios, simple image analysis of results, and the inherent amenability to normalization which minimizes differences of biosensor concentration or experimental set-up from analyses (37, 38).

### **The evolution of FRET-based biosensors for investigating kinase activity in living cells**

FRET-based kinase activity reporters are relatively novel, yet powerful tools for investigating the regulation of kinases in their natural biological context. Described below are examples on the evolution of such biosensors that have been used for studying two key kinases, ERK and PKA, which are involved in a number of cellular signaling processes.

### **Extracellular signal-regulated kinase (ERK)**

The first FRET-based biosensor designed for measuring the activity of ERK, Miu2, was developed in 2006 by Matsuda and collaborators (30). The biosensor was composed of the fluorescent proteins CFP and YFP flanking, yet spaced with short amino acid linkers, an endogenous ERK2 protein. The biosensor utilized the conformational change of ERK upon binding of its activator, MEK, to bring the FRET pair closer spatially and increase the FRET signal. However, this design suffered from the disruption of normal cell activities caused by the overexpression of total cellular ERK2, and that it did not fully reflect ERK activity. In 2007, these issues were addressed by a new design, Erkus, which was developed in the lab of Y. Umezawa (39). Instead of utilizing endogenous ERK, a short yet specific target substrate of ERK, Threonine 669 within the epidermal growth factor receptor, and a threonine phosphoamino acid domain, Forkhead-Associated 2 (FHA2), served as a molecular switch to sense ERK activity. Flanked by the same CFP/YFP FRET pair, the molecular switch would undergo a conformational change that would increase the FRET signal upon substrate phosphorylation and the subsequent recognition and binding by the FHA2 domain. A more recent biosensor, EKAR, designed by Svoboda and collaborators utilized improvements in fluorescent protein technology for new FRET pairs and adaptations to the other components of the biosensor (29). The novel molecular switch components of EKAR are composed of a shortened Cdc25C substrate domain containing the ERK-phosphorylatable Thr48 residue, and a WW phosphoamino acid binding domain that has increased affinity for the phosphorylated substrate. Moreover, the two domains were separated by a 72-glycine linker to improve the flexibility and folding of the biosensor. The EKAR biosensor has a higher dynamic



range, roughly 20 percent, compared to previous ERK biosensors and has been a powerful tool for studying ERK signaling dynamics in neuronal cells (29, 40).

Most recently, EKAR and a number of other kinase reporters were optimized for FRET using an optimized backbone developed by Matsuda and collaborators (25). This backbone consists of repeats of the amino acid sequence SAGG to serve as a flexible linker flanked on one side by the phosphoamino acid binding domain attached to one FP and on the other side by the kinase substrate attached to the other FP. This linker is claimed to render the biosensors solely distance-dependent and allow for enhanced signal-to-noise ratios and improved FRET gain, defined as the relative change in the FRET ration after stimulation compared to the value before stimulation. Thus, the linkers were named EeVee linkers for their enhancement of visualizing biochemical events by evading extra FRET (25).

### **cAMP- dependent protein kinase (PKA)**

The first FRET-based biosensor of PKA activity, ART, was published in 2000 by Hagimara et al (41). It contains a kinase inducible domain of the cAMP-responsive element-binding protein (CREB) that is flanked by the FRET pair BGFP and RGFP. Upon phosphorylation by PKA, the kinase inducible domain undergoes a conformational change that distances the fluorescent proteins and thus disrupts the FRET signal. This sensor however, suffered from the poor photostability of the fluorescent proteins and only modest changes in the FRET signal upon PKA phosphorylation. These shortcomings were addressed by the AKAR biosensor developed by Zhang and collaborators (31). The first generation of AKAR has a similar design to most other FRET biosensors and is

composed of a 14-3-3 $\tau$  phosphoamino acid binding domain and a modified PKA substrate, kemptide, flanked by the improved fluorescent proteins, enhanced cyan and citrine. The second generation of this sensor utilized a lower affinity molecular switch composed of a FHA1 phosphoamino acid domain and a different substrate to improve the reversibility of the sensor (42). These biosensors were crucial for investigation of the compartmentalized modulation of PKA and the effects of substrate tethering, as well as the role of phosphatases in signaling complexes mediated by A-kinase anchoring proteins.

### **Computational and systematic modeling using fluorescent microscopy data**

Signaling pathways are often large networks composed of a number of nodes, each of which can be modulated by complex interactions with components of other pathways through crosstalk. As such, traditional molecular biology techniques utilized have been successful for investigating the functions of individual components and for qualitatively describing how signaling pathways occur. Yet, a great deal of information lies in how each component interacts in the network as whole and what systems-level properties allow for the finer tuning of signal transduction processes. FRET-based kinase reporters benefit modeling approaches with data on the kinetics of activity and spatial dynamics of kinases in their native biological context. One recent example of the power of this combination utilized fluorescence microscopy using the EKAR biosensor expressed in fibroblasts for developing a model to account for ERK phosphorylation, localization, and activity in response to growth factor stimulation (43). The experimentally verified results show that active, free ERK in the nucleus temporally lags

nuclear translocation and it is suggested that substrate interactions act as a temporal buffer. The fit model suggests that as ERK accumulates in the nucleus, active ERK is initially buffered by interactions with nuclear targets and protected from deactivation by phosphatases. The results of this study display the capacity of utilizing FRET-based imaging with computational modeling for providing greater insight into signaling mechanisms.

### **Expanding biosensors for new applications**

Continuing advancements in fluorescent protein technology and microscopy techniques will allow for improved FRET-based biosensors and further complement the study of signaling dynamics in living cells. Moreover, enhancements made to these biosensors will continue to benefit diverse biomedical applications. Described herein are a number of investigations aimed to optimize and expand the versatility of the FRET-based EKAR-EV biosensor to further understand the spatiotemporal dynamics and regulation in the ERK signaling pathway. Such and continued improvements will allow for finer detection of biochemical events and allow for an increased understanding of cell signaling dynamics and cell fate decisions.

## References

1. van der Geer, P., Hunter, T., and Lindberg R.A. (1994) *Annu. Rev. Cell Biol.* 10, 251-337.
2. Manning, G., Whyte, D.B., Martinez, R., Hunter, T., and Sudarsanam, S. (2002) *Science* 298, 1912-1934.
3. Hanks, S.K. (2003) *Genome Biol.* 4, 111.
4. Zhang, J., Yang, P.L., and Gray N.S. (2009) *Nat. Rev. Cancer* 9, 28-39.
5. Ma, H., Deacon, S., and Horiuchi, K. (2009) *Expert Opin. Drug Discov.* 3, 607-621.
6. Jia, Y., Quinn, C.M., Kwak, S., and Talanian, R.V. (2008). *Curr. Drug Discov. Technol.* 5, 59-69.
7. Ni, Q., Titov, D.V., and Zhang, J. (2006) *Methods* 40, 279-286.
8. Kalab, P. and Soderholm, J. (2010) *Methods* 51, 220-232.
9. Förster, T. (1948). *Ann. Phys.* 2, 55-75.
10. Zadran, S., Standley, S., Wong, K., Otiniano, E., Amighi, A., and Baudry M. (2012) *Appl. Microbiol. Biotechnol.* 96, 895-902.
11. Zhou, X., Herbst-Robinson, K.J., and Zhang, J. (2012) *Methods Enzymol* 504, 317-340.
12. Lakowicz, J.R. (2006) *Principles of Fluorescence Spectroscopy*, Springer Science, New York, 2006.
13. Kremers, G., Gilbert, S.G., Cranfill, P.J., Davidson, M.W., and Piston, D.W. (2011) *J Cell Sci.* 124, 157-160.
14. Shaner, N. C., Steinback, P. A., and Tsien, R. Y. (2005) *Nat. Methods* 2, 905-909.
15. Shaner, N. C., Lin, M. Z., McKeown, M. R., Steinbach, P. A., Hazelwood, K. L., Davidson, M. W. and Tsien, R.Y. (2008) *Nat. Methods* 5, 545-551.
16. Tsien, R. Y. (1998) *Annu. Rev. Biochem.* 67, 509-544.
17. Pedelacq, J.-D., Cabantous, S., Tran, T., Terwilliger, T. C. and Waldo, G. S. (2006) *Nat. Biotechnol.* 24, 79-88.
18. Griesbeck, O., Baird, G. S., Campbell, R. E., Zacharias, D. A. and Tsien, R. Y. (2001) *J. Biol. Chem.* 276, 29188-29194.
19. Kimata, Y., Iwaki, M., Lim, C. R. and Kohno, K. (1997) *Biochem. Biophys. Res. Commun.* 232, 69-73.

20. Subach, F. V., Subach, O. M., Gundorov, I. S., Morozova, K. S., Piatkevich, K. D., Cuervo, A. M. and Verkhusha, V. V. (2009) *Nat. Chem. Biol.* 5, 118-126.
21. Goedhart, J., van Weeren, L., Hink, M. A., Vischer, N. O. E., Jalink, K. and Gadella, T. W. J. (2010) *Nat. Methods* 7, 137-139.
22. Kohl, T., Heinze, K.G., Kuhlemann, R., Koltermann, A., and Schwille, P. (2002) *Proc. Natl. Acad. Sci. U.S.A.* 99, 12161-12166.
23. Ai, H.W., Hazelwood, K.L., Davidson, M.W., and Campbell, R.E. (2008) *Nat Methods* 5, 401-403.
24. Zhang, J. and Allen, M.D. (2007) *Mol Biosyst* 3, 759-765.
25. Komatsu, N., Aoki, Y., Yamada, M., Yukinaga, H., Fujita, Y., Kamioka, Y., Matsuda, M. (2011) *Mol Biol Cell* 22, 4647-4656.
26. Constantinou, A. and Polizzi, K.M. (2013). *Biochem Soc Trans* 41, 1146-1151.
27. Zhang, J., Campbell, R.E., Ting, A.Y., and Tsien, R.Y. (2002) *Nat. Rev. Mol. Cell Biol.* 3, 906-918.
28. Ni, Q., Ganesan, A., Aye-Han, N.N., Gao, X., Levchenko, A., and Zhang, J. (2011) *Nat. Chem. Biol.* 7, 34-40.
29. Harvey, C.D., Ehrhardt, A.G., Cellurale, C., Zhong, H., Yasuda, R., Davis, R.J., and Svoboda, K. (2008). *Proc. Natl. Acad. Sci. U.S.A.* 105, 19264-19269.
30. Fujioka, A., Terai, K., Itoh, R.E., Aoki, K., Nakamura, T., Kuroda, S., Nishida, E., and Matsuda, M. (2006) *J. Biol. Chem.* 281, 8917-8926.
31. Zhang, J., Ma, Y., Taylor, S.S., and Tsien, R.Y. (2001) *Proc. Natl. Acad. Sci. U.S.A.* 98, 14997–15002.
32. Aye-Han, N.N., Allen, M.D., Ni, Q., and Zhang, J. (2012). *Mol. Biosyst* 8, 1435-1440.
33. Fosbrink, M., Aye-Han, N.N., Cheong, R., Levchenko, A., and Zhang, J. (2010) *Proc. Natl. Acad. Sci. U.S.A.* 107, 5459-5464.
34. Liao, X., Lu, S., Zhuo, Y., Winter, C., Xu, W., and Wang, Y. (2012) *PLoS. One* 7, e42709.
35. Wang, Y., Botvinick, E. L., Zhao, Y., Bems, M. W., Usami, S., Tsien, R. Y., and Chien, S. (2005) *Nature* 434, 1040-1045.
36. Bogoyevitch, M.A. and Kobe, B. (2006) *Microbiol. Mol. Biol. Rev.* 70, 1061-1095.
37. Miyawaki, A. (2003) *Dev. Cell* 4, 295-305.
38. Carlson, H.J. and Campbell, R.E. (2009) *Curr. Opin. Biotechnol.* 20, 19-27.
39. Sato, M., Kawai, Y., and Umezawa, Y. (2007) *Anal. Chem.* 79, 2570–2575.

40. Zeiller, C., Blanchard, M.P., Pertuit, M., Thirion, S., Enjalbert, A., Barlier A., and Gerard, C. (2012) *Cell. Signal.* 24, 2237-2248.
41. Nagai, Y., Miyazaki, M., Aoki, R., Zama, T., Inouye, S., Hirose, K., Iino, M., and Hagiwara, M. (2000) *Nat. Biotechnol.* 18, 313-316.
42. Zhang, J., Hupfeld, C.J., Taylor, S.S., Olefsky, J.M., and Tsien, R.Y. (2005) *Nature* 437, 569-573.

# **Chapter 1**

## **Optimization of FRET-based Biosensor for Investigation of Extracellular Signal-Regulated Kinase Dynamics**

## **ERK-MAPK signaling**

Cells require a number of strictly regulated mechanisms such that signal transduction pathways are regulated in time and space to sense and appropriate distinct responses to a plethora of environmental stimuli. One notable example of the importance of such regulation in response to various extracellular signals is the extracellular-signal-regulated kinases (ERKs), which regulate cell cycle progression, differentiation, and apoptosis. ERK signaling can be activated by a number of stimuli, including growth factors, cytokines, and carcinogens, to dictate various cellular fates. As a component of one of the four canonical mitogen-activated protein kinase (MAPK) cascades, ERK1/2 is activated in three-tiered protein kinase cascade that is stimulated by the binding of a ligand to its respective receptor, receptor tyrosine kinases, G-protein coupled receptors, and ion channels. Upon binding of a growth factor, phosphorylation of tyrosine residues on the cytoplasmic receptor domain facilitates signaling through adaptor proteins that mediate the localization of a guanine nucleotide exchange factor, son of sevenless (SOS). SOS facilitates the exchange of GDP for GTP on Ras GTPases resulting in a conformational change of Ras that allows for plasma membrane recruitment and activation of its effectors, including Raf-family kinases. The activated Raf kinase, a MAPKKK phosphorylates a dual-specificity MAPKK, MAPK Kinase, which in turn phosphorylates a MAPK, such as ERK. A representative diagram of this signaling cascade is shown in Figure 1.1.



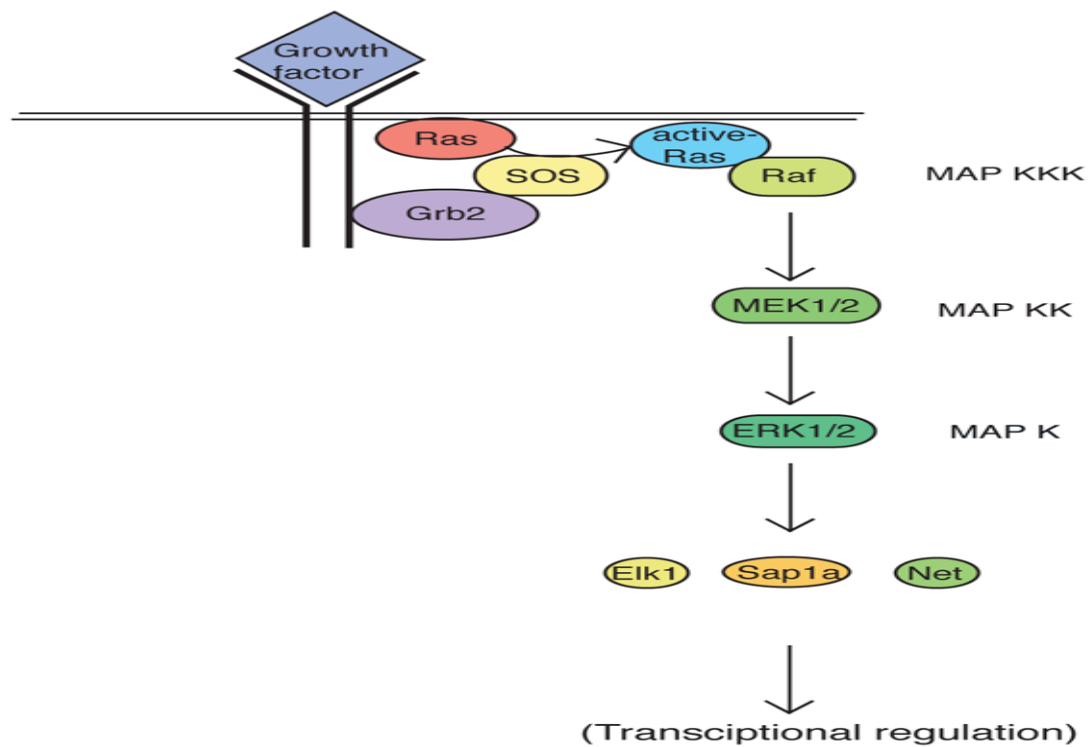


**Figure 1.1:** ERK-MAPK cascade. Growth factor binding causes a conformational change in the receptor tyrosine kinase and phosphorylation of tyrosine residues on the cytoplasmic receptor domain. Phosphorylated tyrosine residues facilitate signaling through adaptor proteins that which bind and localize guanine nucleotide exchange factor, son of sevenless (SOS) to the plasma membrane. SOS facilitates the exchange of GDP for GTP on Ras GTPases resulting in a conformational change of Ras that allows for plasma membrane recruitment and activation of its effectors, including Raf-family kinases. This initiates the MAPK cascade through subsequent activation of MEK and then ERK. Figure from RIKEN Bioresource center<sup>1</sup>.

<sup>1</sup>[http://dna.brc.riken.jp/en/GENESETBANK/0200104Erk\\_cascade\\_2.html](http://dna.brc.riken.jp/en/GENESETBANK/0200104Erk_cascade_2.html)

Such a cascade not only allows for signal amplification, where each upstream component can act on several downstream targets, but also adds regulatory interfaces for the fine tuning of kinetics, duration, and amplitude of the signaling system. ERK is positively regulated through phosphorylation by the dual-specificity mitogen activated ERK kinases, MEK1 and MEK2. Upon MEK-mediated phosphorylation of ERK1 on the Threonine 202 and Tyrosine 204 residue and of ERK2 on the Threonine 185 and Tyrosine 187 residues, the kinase activities of ERK are activated (1). Phosphorylated ERK can dimerize into primarily ERK1 and ERK2 homodimers. This dimerization is believed to enhance ERK activity levels and also play a role in ERK translocation to the nucleus (2, 3). Activated ERKs are serine/threonine kinases that can directly and indirectly phosphorylate and activate a number of downstream targets that span different subcellular compartments (4).

Active ERK is known to phosphorylate at least 150 known protein substrates, approximately equally located in both the cytoplasm and nucleus (5). In quiescent cells, activated ERK is primarily localized in the cytoplasm. The cytoplasmic targets of ERK include a number of components of various pathways that are phosphorylated directly by ERK and result in the negative feedback regulation of ERK activity. ERK phosphorylation of multiple residues on Son of Sevenless (SOS), a guanine nucleotide exchange factor, results in inhibition of Ras activation (6). Furthermore, direct-ERK phosphorylation of EGF receptors, and phosphorylation-dependent inhibition of the degradation of MAPK-specific phosphatases are also involved in the negative feedback of ERK (7, 8).

The activation of ERK also can result in its release from scaffold proteins in the cytoplasm and its rapid translocation to the nucleus by both passive and energy-dependent mechanisms (9-11). While previously thought to be solely due to dimerization of ERK, passive energy-independent translocation is increasingly believed to be controlled by its rate of activation by MEK (10). Shuttling of ERK to the nucleus is vital for growth factor-induced changes in gene expression and DNA replication, as ERK directly phosphorylates a number of transcription factors, including its most characterized substrate, Elk1. Moreover, ERK activity in the nucleus can indirectly activate other transcription factors through its phosphorylation of a family of RSK-related kinases, Mitogen- and stress-activated protein kinases (MSKs), whose transcription factor substrates include ATF1, CREB, and HMG14. The translocation of activated ERK in the nucleus is balanced by deactivating phosphatases and by export to the cytoplasm.

### **Regulation of ERK activity and specificity**

While ERK is regulated by a number of kinases, other than MEK1 and MEK2, as well as a variety of phosphatases, such regulatory mechanisms cannot account for the large number and often opposing outcomes induced by ERK. The ability of this seemingly linear cascade to result in many distinct effects induced by a variety of stimulations has drawn much attention to the regulation mechanisms that allow for ERK signaling specificity. The elucidated mechanisms are listed and subsequently described as follows:

1. control on the duration and amplitude of ERK activity;
2. interactions with scaffold proteins to form multicomponent complexes;
3. crosstalk with components of other

pathways that are simultaneously activated; and 4. compartmentalization of MAPK cascade components and targets.

While ERK substrates are differentially expressed in a cell-type specific manner, activation of specific substrates relies on a threshold effect (12). Thus, the control on the period and amplitude of ERK activity is pivotal in signal integration. Differences in the duration and strength of ERK activity were observed in PC12 cells, in which EGF and NGF activation resulted in distinct outcomes. EGF stimulation led to transient activation of ERK and cell proliferation, whereas NGF stimulation resulted in sustained ERK activation and differentiation (13). These differences are attributed to NGF's activation of another GTPase, Rap1, that is also capable of activating Raf, and thus allowing for sustained ERK activation (14). The effects of signal length are believed to occur through immediate early genes that induce a variety of cellular processes (15).

Scaffold proteins assemble multicomponent complexes of often consecutive components to facilitate the kinetics, strength, and specificity of signaling cascades. Moreover, scaffold proteins have an important role in the spatial distribution and spatial selectivity of signals. In resting cells, ERK is primarily retained in the cytoplasm by interactions with such scaffolds through a cytosolic retention sequence/common docking (CRS/CD) domain. ERK interacts with anchoring proteins, such as MEK (16), KSR (17), and PTP-SL (18), and dissociate in a stimulus-dependent manner caused by activation-induced conformational changes (19). Moreover, ERK interactions with other scaffold proteins, such as MP1(20) and VDAC(21), can also direct ERK to endosomal and mitochondrial cellular compartments, respectively. The effects of scaffold proteins add another level of complexity to the fine-tuning of ERK regulation.

While the ERK MAPK cascade is a central signaling pathway, other pathways, including PI3K-AKT, can be activated by the same stimulation and affect the ERK cascade. Through crosstalk, cascade components can interact and thereby modulate the activity of each other and result in combinatorial downstream effects (22). As an example, PI3K has been shown to have a role in the activation of Ras through direct interaction (23).

Realizing the complexity of the regulation of ERK signaling occurring in both time and space within a cell, furthering our understanding necessitates methods that allow for simultaneously measuring spatial and temporal activity of ERK in its natural biological context. The genetically-encodable FRET-based ERK activity reporter, EKAR, has been instrumental in meeting the needs for such investigation. However, this and other FRET-based biosensors can be further optimized to provide greater dynamic ranges and allow for the detection of smaller amplitude and transient biochemical events, particularly necessary for the study of spatio-temporal signaling dynamics (24).

### **Optimization of EKAR**

Literature on the recent evolution of EKAR demonstrates that utilization of different phosphoamino acid binding domains, ERK substrate domains, and linkers between the two former domains have allowed for improvements in the dynamic range of the ERK activity biosensor. The most recent and significant modification is the substitution of the original glycine linker in EKAR with the flexible EeVee-linker to generate EKAREV. This modification roughly tripled the dynamic range of the sensor (25). The dynamic range is defined as the relative change in the normalized FRET

emission ratio (FRET/Donor) after stimulation and is given as a percentage of the basal FRET emission ratio. The 116 amino acid length of EeVee-linker for EKAR was optimized to reduce basal, pre-stimulation FRET signals, maximize dynamic range, and is thought to render EKAR FRET to be solely distance dependent due to the flexible nature of the linker. However, as described in the introduction, FRET efficiency is a function of many variables and is largely influenced by both the relative orientation and the distance between two fluorophores. As a means to examine if the intramolecular FRET of the EKAR-EV sensor is truly independent of the orientation of the fluorophores, EKAR2.3 was constructed by to alter the fluorophore orientation by swapping the order of the FPs in EKAR-EV. EKAR2.3 has minor differences in restriction endonuclease cut-sites between each of the sensor's domains and has the reverse order of fluorescent proteins (with N-terminal ECFP and C-terminal YPet) in the sensor, compared to EKAREV (with N-terminal YPet and C-terminal ECFP). As a control, EKAR2.0, which has a similar order of FPs to EKAR-EV, but with the same set of cut-sites as EKAR2.3, was constructed. Under the hypothesis that the dynamic range would be significantly different when swapping the order of the FPs if the intramolecular FRET of EKAR-EV is dependent on fluorophore orientation, characterization of these probes were conducted in HEK293 cells stimulated with EGF. Interestingly, this simple modification nearly doubled the dynamic range of the sensor (Figures 1.2-1.3).

EKAR-EV-NES	YPet	WW(1-54)	EV29	Cdc25C, DD	ECFP
EKAR 2.3-NES	ECFP	WW(1-54)	EV29	Cdc25C, DD	YPet
EKAR 2.0-NES	YPet	WW(1-54)	EV29	Cdc25C, DD	ECFP

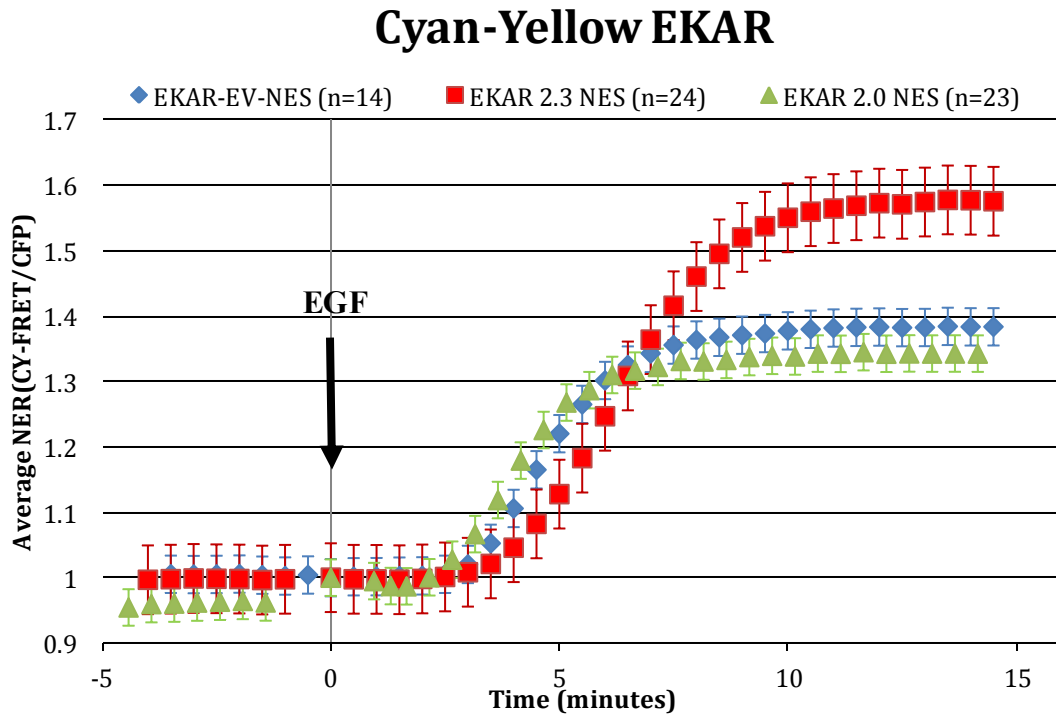


**Figure 1.2:** Average EGF-induced responses of cyan-yellow EKARs. Mean-value responses of cytoplasmic-targeted EKARs with a C-terminal nuclear exclusion sequence (NES) in HEK293 cells stimulated by 100 ng/mL EGF.

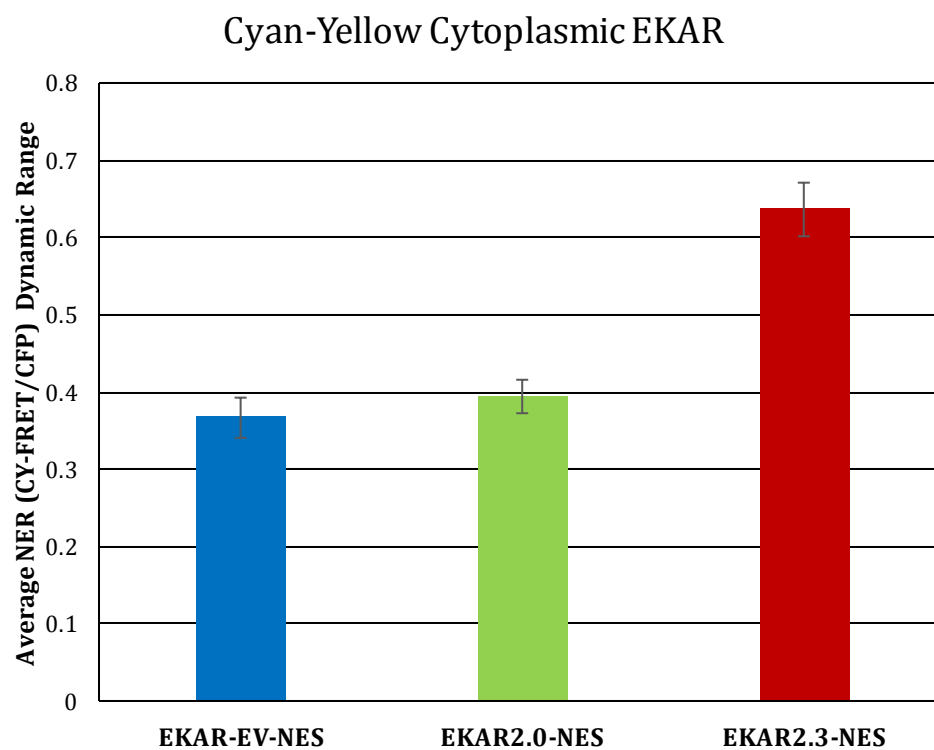


**Figure 1.3:** Average dynamic ranges of cytoplasmic-targeted cyan-yellow EKARs.

Responses in HEK293 cells stimulated by 100 ng/mL EGF.



The results suggest that FRET efficiency and thus dynamic range of EKAR is indeed dependent on the fluorophore orientations with the EeVee linker. Yet, the question is raised whether the developed EKAR2.3 with the reverse order of FPs will show a similar decreasing trend in dynamic with decreasing lengths of the EeVee linker. If this trend holds for EKAR2.3, this result would suggest the necessity of the dual optimization of EeVee-based biosensors for both distance and orientation to achieve the desired optimization for the maximization of the sensor's dynamic range.

To address this question, the effects of different lengths of the EeVee linker in the EKAR2.3 biosensor on the EGF-induced responses in HEK293 cells are examined. The EeVee linker length of 116 amino acids for EKAREV was optimized for the ECFP/YPet FRET pair in a particular orientation. Under the assumption that the fluorophore orientation is independent of fluorophore distance using this flexible linker, it would be expected that shorter EeVee linker lengths in EKAR2.3 would show a similar trend to the dynamic range shown for EKAREV. That is, shorter EeVee linker lengths in EKAR2.3 would result in decreasing the dynamic range of the sensor.

Using EKAR2.3 with a 116 amino acids EeVee linker as a template, two variants of the sensor with EeVee linker lengths of 54 (EKAR2.2) and 36 amino acids (EKAR 2.1) were developed and characterized. As shown in Figure 1.4, decreasing the length of the linker causes an attenuation of the dynamic range of the sensor, defined as the relative change in the normalized FRET ratio after stimulation as a percentage from 63.3 +/- 1.3% for EKAR 2.3 to 51.8 +/- 4.9% for EKAR2.1.

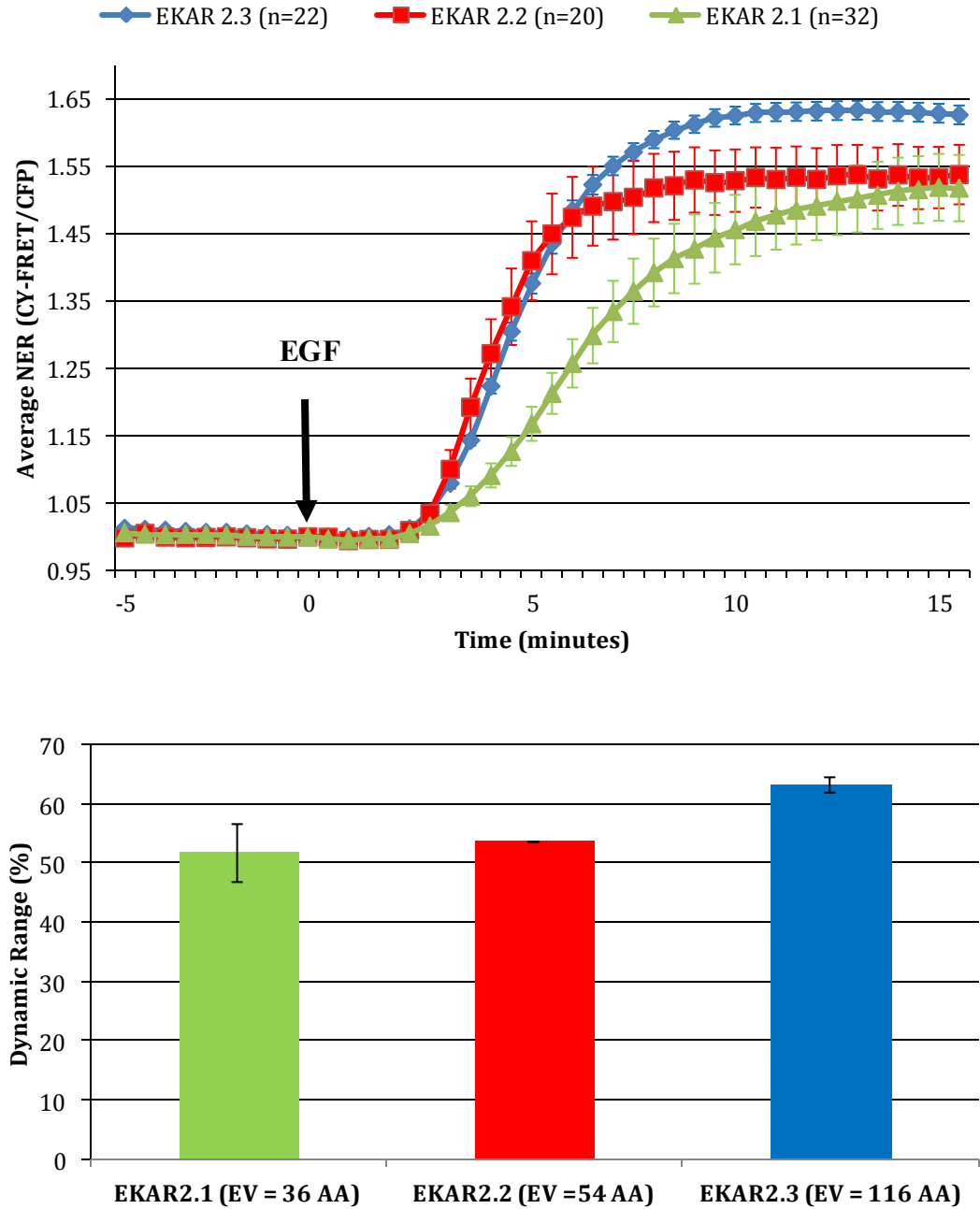


**Figure 1.4:** Effects of EeVee linker length on EKAR dynamic range. (Top) Average Cyan-Yellow EKAR response time course, with EeVee linkers lengths ranging from 36 to 116 amino acids (AA), in HEK293 cells stimulated by 100 ng/mL EGF. (Bottom) Average Cyan-Yellow EKAR dynamic ranges.

Conceptually, the attenuation of the dynamic range of the sensor with shorter EeVee linker lengths is best explained by evaluation of the basal FRET ratios (25). By elongating the distance between the two FPs, the basal FRET values decrease due to the longer separation in space between the FRET pair. As shown in Figure 1.5, the reverse FP order EKAR, ECFP-Sensor-YPet, shows a similar trend in the decrease of basal FRET ratios with elongation of the EeVee linker, compared to the previously reported EKAR-EV probe, YPet-Sensor-ECFP (25).

Our results suggest that the optimization of EeVee based FRET biosensors requires attention for the effects of orientation on the dynamic range of the probe. While previously thought that the flexible EeVee linker would render the effects of orientation negligible for efficient FRET, we find that reversing the order of the fluorescent proteins in EKAR significantly enhances the dynamic range of the probe. Moreover, we find that for the new configuration of the EKAR probe that reducing the length of the EeVee linker significantly reduces the dynamic range of the probe, as was also observed for the original configuration. Thus, we conclude that the EKAR probe requires a dual optimization routine for EeVee linker length and to account for fluorophore orientation. This conclusion can likely be extended to other EeVee-based biosensors. Further efforts to improve the dynamic range of this and other probes will provide great benefit to the detection and characterization of small amplitude and transient biochemical activities.

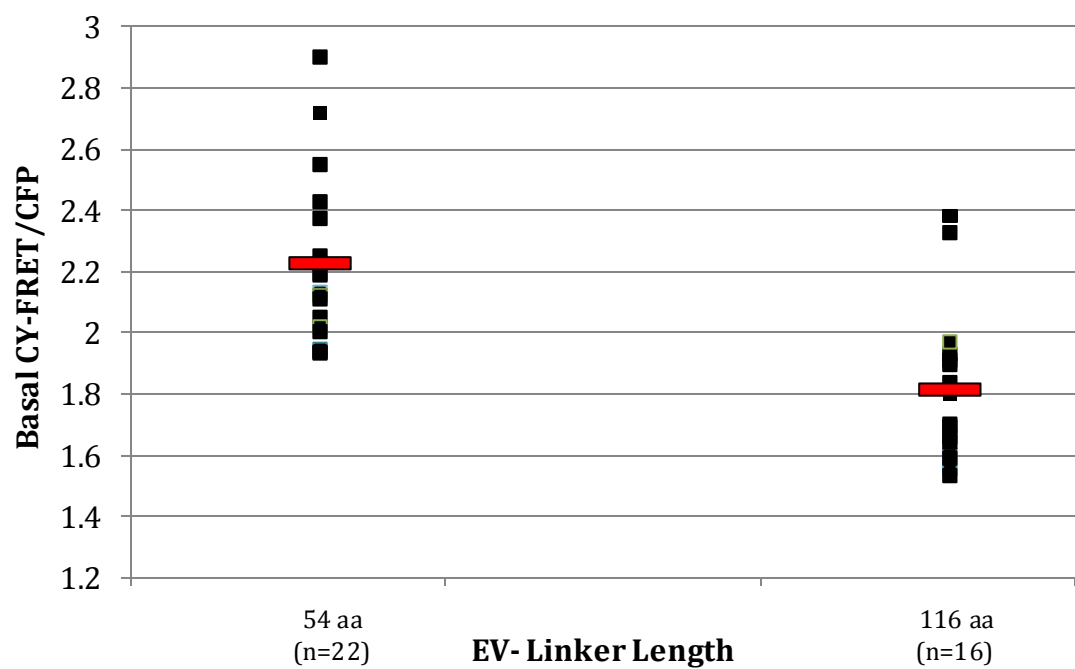


**Figure 1.5:** Effects of EeVee linker length on EKAR basal FRET values. Basal non-normalized FRET values are shown for each cell (black square) in HEK293 cells. The average basal FRET value is shown by the red bar.

## Methods

**Gene construction of EKAR.** Cyan and yellow fluorescent proteins [ECFP, YPet] were PCR amplified with the appropriate restriction digest sites for incorporation into EKAR2.3 by replacing the ECFP or YPet fluorescent proteins. To generate EKAR with modified EeVee linker lengths, the sensor region of the probe was PCR amplified and selected for length for reincorporation into the plasmid. The EKAR constructs were generated in pRSET B (Invitrogen) and then subcloned to pcDNA3 (Invitrogen) after a Kozak sequence for high-level, stable, and transient expression in mammalian cells.

**Cell culture and imaging.** HEK-293 cells were plated on sterilized glass coverslips in 35-mm dishes and grown to ~50% confluency in Dulbecco's modified eagle medium (DMEM) with 10% Fetal bovine serum (FBS) at 37°C and 5% CO<sub>2</sub>. Cells were transfected with Lipofectamine2000 and allowed to grow 20-24 hours before imaging. After washing twice with Hanks' balanced salt solution, cells were maintained in buffer for the duration of the experiments. PC12 cells were plated on sterilized glass coverslips in 35-mm dishes and grown to ~50% confluency in DMEM with 10% (FBS) and 5% Donor horse serum (DHS) at 37°C and 5% CO<sub>2</sub>. Human epidermal growth factor (Human EGF), and U0126 (Sigma) were utilized as indicated.

Imaging experiments were conducted on a Zeiss Axiovert 200M microscope with a 40x/1.3NA oil-immersion objective and cooled charge-coupled-device camera (MicroMAX BFT512; Roper Scientific, Trenton, NJ) controlled by METAFLUOR software (Molecular Devices, Sunnyvale, CA). Dual emission CFP/YFP ratio imaging required a 420DF20 excitation filter, 475DF40 and 535DF25 emission filters, for CFP

and YFP respectively, and a 600DRLP dichroic mirror. Raw fluorescent images were reanalyzed and corrected using the METAFLUOR software and MATLAB (MathWorks Inc., Natick, MA) to subtract background fluorescent and for normalization by the basal emission ratios, such that the emission ratios before drug stimulation are set with a value of unity.

## References

1. Xu, S., Robbins, D., Frost, J., Dang, A., Lange-Carter, C., and Cobb, M.H. (1995) *Proc. Natl. Acad. Sci. U.S.A.* 92, 6808–6812.
2. Philipova, R. and Whitaker, M. (2005) *J. Cell Sci.* 118, 5767–5776.
3. Burack, W.R. and Shaw, A.S. (2005) *J. Biol. Chem.* 280, 3832-3837.
4. Thomas, G.M. and Huganir, R.L. (2004) *Nat. Rev. Neurosci.* 5, 173-183.
5. Yoon, S. and Seger, R. (2006) *Growth Factors* 24, 21-44.
6. Chen, D., Waters, S.B., Holt, K.H., Pessin, J.E. (1996) *J. Biol. Chem.* 271, 6328-6332.
7. Li, X., Huang, Y., Jiang, J., and Frank, S.J. (2008) *Cell Signal.* 20, 2145-2155.
8. Peng, D.J., Zhou, J.Y., and Wu, G.S. (2010) *Cell Cycle* 9, 4650-4655.
9. Burack, W.R. and Shaw, A.S. (2005) *J. Biol. Chem.* 280, 3832-3837.
10. Lidke, D.S., Huang, F., Post, J.N., Rieger, B., Wilsbacher, J., Thomas, J.L., Pouyssegur, J., Jovin, T.M., and Lenormand, P. (2010) *J. Biol. Chem* 285, 3092-3102.
11. Marchi, M., Parra, R., Costa, M., and Ratto, G.M. (2010) *Method Mol. Biol.* 661, 287-301.
12. Chambard, J., Lefloch, R., Pouyssegur, J., Lenormand, P. (2007) *Biochim. Biophys. Acta Mol. Cell Res.* 1773, 1299-1310.
13. Nguyen, T.T., Scimeca, J.C., Filloux, C., Peraldi, P., Carpentier, J.L., and Van Obberghen, E. (1993) *J. Biol. Chem.* 268, 9803-9810.
14. Sasagawa, S., Ozaki, Y., Fujita, K., and Kuroda, S. (2005) *Nat. Cell Biol.* 7, 365-373.
15. Murphy, L.O., MacKeigan, J.P., and Blenis, J. (2004) *Mol. Cell Biol.* 24, 144-153.
16. Fukuda, M., Gotoh, Y., and Nishida, E. (1997) *EMBO J.* 16, 1901–1908.
17. Morrison, D. K., and Davis, R. J. (2003) *Annu. Rev. Cell Dev. Biol.* 19, 91–118.
18. Blanco-Aparicio, C., Torres, J., and Pulido, R. (1999) *J. Cell Biol.* 147, 1129–1136.

19. Wolf, I., Rubinfeld, H., Yoon, S., Marmor, G., Hanoch, T., and Seger, R.  
(2001) *J. Biol. Chem.* 276, 24490–24497.
20. Wunderlich, W., Fialka, I. Teis, D., Alpi, A., Pfeifer, A., Partron, R.G., Lottspeich, F., and Huber, L.A. (2001) *J. Cell Biol.* 152, 765-776.
21. Galli, S., Jahn, O., Hitt, R., Hesse, D., Opitz, L., Plessmann, U., Urlaub, H., Poderoso, J.J., Jares-Erijman, E.A., and Jovin, T.M. (2009) *PLoS One.* 4, e7541.
22. Shaul, Y.D. and Seger, R. (2007) *Biochim. Biophys. Acta.* 1773, 1213-1226.
23. Wennstrom, S. and Downward, J. (1999) *Mol. Cell Biol.* 19, 4279-4288.
24. Lam, A., St-Pierre, F., Gong, Y., Marshall, J.D., Cranfill, P.J., Baird, M.A., McKeown, M.R., Wiedenmann, J., Davidson, M.W., Schnitzer, M.J., Tsien, R.Y., and Lin, M.Z. (2012) *Nat. Methods* 9, 1005-1012.
25. Komatsu, N., Aoki, Y., Yamada, M., Yukinaga, H., Fujita, Y., Kamioka, Y., and Matsuda, M. (2011) *Mol Biol Cell* 22, 4647-4656.



## **Chapter 2**

### **Expansion of the Application of EKAR for Investigation of Extracellular Signal-Regulated Kinase Dynamics**

## **Development and Characterization of EKAR color variants**

With the ongoing advancements in the fluorescent protein (FP) technology that provide novel FP variants with a wide array of spectral profiles and properties (1, 2), FRET-based biosensors can continue to be engineered for a variety of experimental purposes and for improvements in dynamic range. Having optimized the cyan-yellow version of EKAR with an EeVee linker for dynamic range, we now shift focus to expanding the application of this sensor to address questions on the spatio-temporal regulation and crosstalk of Erk.

Utilizing EKAR2.3 as a starting point, a number of diffusible EKAR variants were generated (Figure 2.1) by replacing the ECFP or YPet FPs in the EKAR 2.3 biosensor with another FP color variant. The generation of this set of EKAR variants is motivated by three objectives. First, the generation EKAR variants with different FRET pairs of varying spectral overlap expands the application of EKAR for co-imaging capability with probes for other signaling molecules. Second, the generation of these EKARs allows for the examination of potentially useful FRET pairs for this sensor and the effects on its dynamic range. Lastly, the subsets of the EKARs that contain the same FPs, but with reverse order allow for a further investigation of the fluorophore orientation dependence of EeVee linker based biosensors.

While a great majority of genetically encoded FRET reporters utilize variants of the CFP/YFP donor-acceptor pair since they are an optimal pair for FRET and due to the markedly enhanced sensitivity for FRET-based biosensors (3), a number of aspects of this pair are precarious for an envisioned goal of simultaneous multiplexing of FRET-based biosensors. The capability of visualizing multiple signaling events at the same time

allows for stronger correlation accuracy due to the minimization of sample-to-sample variability. Utilization of multiple FRET-based biosensors in parallel can be limited by fluorescent cross excitation, and bleed-through of emission signals (4). However, advances have brought about FPs with unique excitation and emissions properties that allow for new potentially useful FRET pairs that have more separated excitation and emissions peaks (5). In particular, those with larger stokes shifts, the difference between the maxima band positions of the excitation and emission spectra, are exceptionally well posed to allow for orthogonal readouts when used in tandem with other such FRET pairs (5-7). Thus, avoiding the potential drawbacks of CFP/YFP FRET sensors for such an objective and testing other potentially beneficial FRET pairs serve as an underlying objective for the development of EKAR color variants.

The generated series of EKAR color variants show a broad array of dynamic range. Upon stimulation of HEK-293 cells expressing each biosensor by 100ng/mL epidermal growth factor (EGF), diffusible EKAR variants show a maximum increase in the mean normalized emission ratios (FRET/donor) ranging from 15.5 +/- 3.7 to 62.7 +/- 1.8 % (average  $\pm$  SEM) with similar kinetics. A summary of the characterization results of the developed EKAR color variants is shown in Figure 2.1. Moreover, inhibition of the ERK pathway by U0126, a selective inhibitor of MEK1 and MEK2, resulted in a comparable decrease of the FRET/donor ratio to near but slightly higher than basal levels as seen for EKAREV. Representative curves for a number of the developed EKAR color variants are shown in Figure 2.2. Thus, the developed biosensors are still sensitive for monitoring ERK activity and reversible to also allow for visualization of the actions by

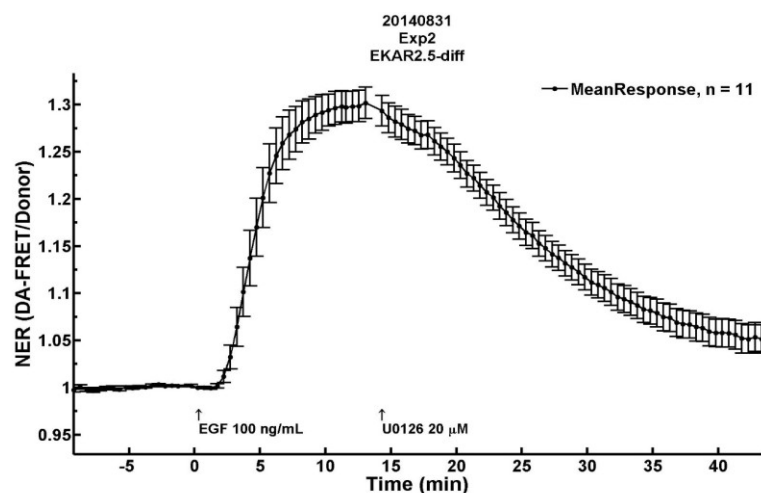
specific phosphatases or other signaling components that inhibit ERK activity. This series EKARs may find unique applications and is the topic of further application.

Construct	EKAR Domain Structure					Mean Response
EKAR 2.3	ECFP	WW(1-54)	EV29	Cdc25C, DD	YPet	62.7 +/- 1.8 % (n= 15)
EKAR 2.4	Cerulean	WW(1-54)	EV29	Cdc25C, DD	YPet	47.7 +/- 2.8 % (n=11)
EKAR 2.5	ECFP	WW(1-54)	EV29	Cdc25C, DD	MCherry	28.9 +/- 4.7 % (n=26)
EKAR 2.6	Cerulean	WW(1-54)	EV29	Cdc25C, DD	MCherry	17.8 +/- 5.5 % (n=11)
EKAR 2.7	MCherry	WW(1-54)	EV29	Cdc25C, DD	YPet	18.4 +/- 5.8 % (n=21)
EKAR 2.8	YPet	WW(1-54)	EV29	Cdc25C, DD	MCherry	15.5 +/- 3.7 % (n=37)
EKAR 2.9	MCherry	WW(1-54)	EV29	Cdc25C, DD	ECFP	45.9 +/- 4.8% (n=14)
EKAR 2.0	YPet	WW(1-54)	EV29	Cdc25C, DD	ECFP	39.2 +/- 5.3% (n=14)

**Figure 2.1:** Design and characterization of diffusible EKAR color variants. Domain structures of developed EKAR biosensors consisting of full length fluorescent protein pairs (ECFP, YPet, Cerulean, or MCherry), a WW phospho-amino acid binding domain, a flexible 116 amino acid EV linker, and an ERK substrate peptide from Cdc25C containing the consensus MAPK target sequence and the ERK specific docking site (DD). Mean maximal responses of HEK-293 cells expressing the EKAR construct stimulated with 100ng/mL epidermal growth factor (EGF).

A

EKAR 2.5



B

EKAR 2.8

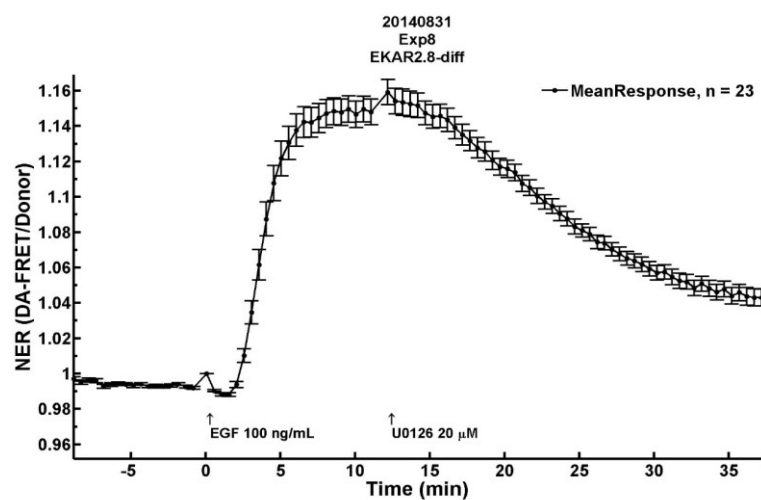
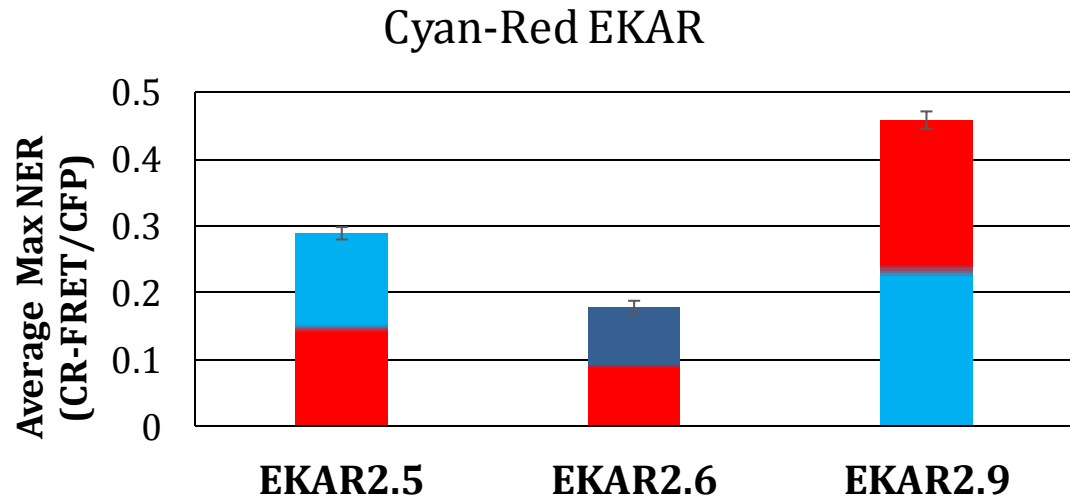


**Figure 2.2:** Representative characterization experiments of EKAR color variants.

Average diffusible responses in HEK293 cells stimulated by 100 ng/mL EGF and 20 $\mu$ M U0126. A) Cyan-Red EKAR2.5 responses. B) Yellow-Red EKAR 2.8 responses.

In line with the conclusion that the EKAREV sensor requires dual optimization of both fluorophore distance, mediated by the length of the EeVee linker, and orientation for a particular FRET pair, it is seen that reversing the order of FPs in the EKAR sensor with the EeVee linker can cause significant changes in the dynamic range. As shown in Figure 2.3, this observation is seen for the Cyan-Red EKAR and for Yellow-Red EKAR, to a lesser extent. These results stress the importance for optimization of both EeVee linker length and fluorophore orientation for each particular FRET pair. Moreover, this result can likely be extended for optimization of the numerous EeVee-based activity reporters that utilize FRET for a number of other kinases.

**A**



**B**

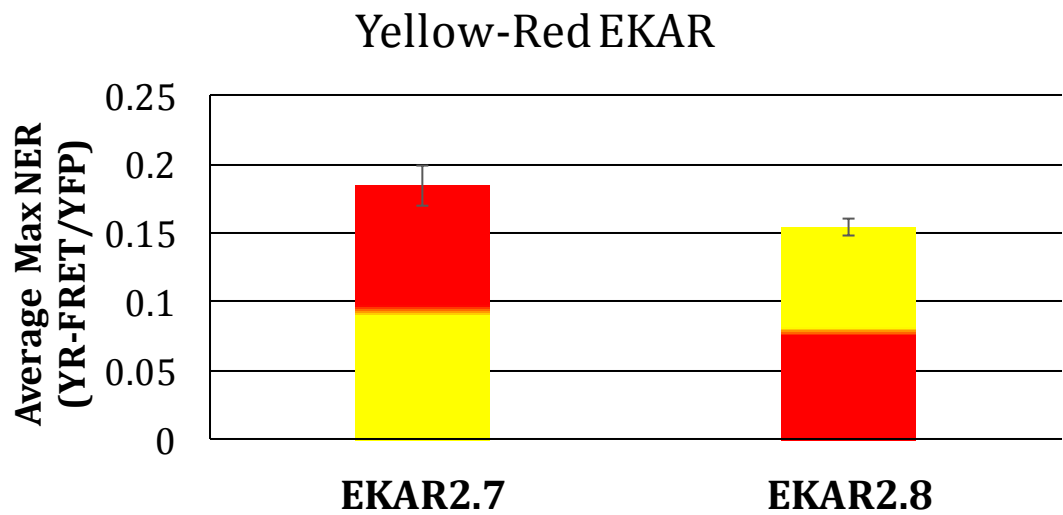


**Figure 2.3:** Average dynamic ranges of diffusible EKAR color variants. Mean-value results of EKAR color variants in HEK293 cells stimulated by 100 ng/mL EGF.

Comparisons for A) Cyan-Red and B) Yellow-Red EKAR variants. Color shading correspond to FP order with the top color representing the N-terminal FP emission color (Light blue: ECFP, Dark Blue: Cerulean, Red: MCherry, and Yellow: YPet).



## **Visualization of ERK activity in the cytoplasm**

A significant advantage of genetically-encoded FRET biosensors is the capability to target them to different subcellular locations via C-terminal localization tags. Cytoplasmic targeting of the EKAR sensor is achieved by tagging the diffusible EKAR construct with a C-terminal nuclear export signal (NES). As shown in Figure 2.4A, HEK293 cells expressing NES-targeted EKAR show strong fluorescence in the cytoplasm with little to no fluorescence in the nucleus. Compared to diffusible EKAR, NES-tagged EKAR shows exclusive localization in the cytoplasm. Contrary to previous reports that targeted localization of FRET-based biosensors can reduce the intrinsic dynamic range of such sensors (8), cytoplasmic localization does not have significant effects on the amplitude or kinetics of the developed EKAR variants (Figure 2.4B). The targeted localization of EKAR provides visualization of ERK activity dynamics in different compartments of the cell. Utilization of targeted versions of the developed EKAR color variants provides a useful application for simultaneously investigating ERK activity in different regions.

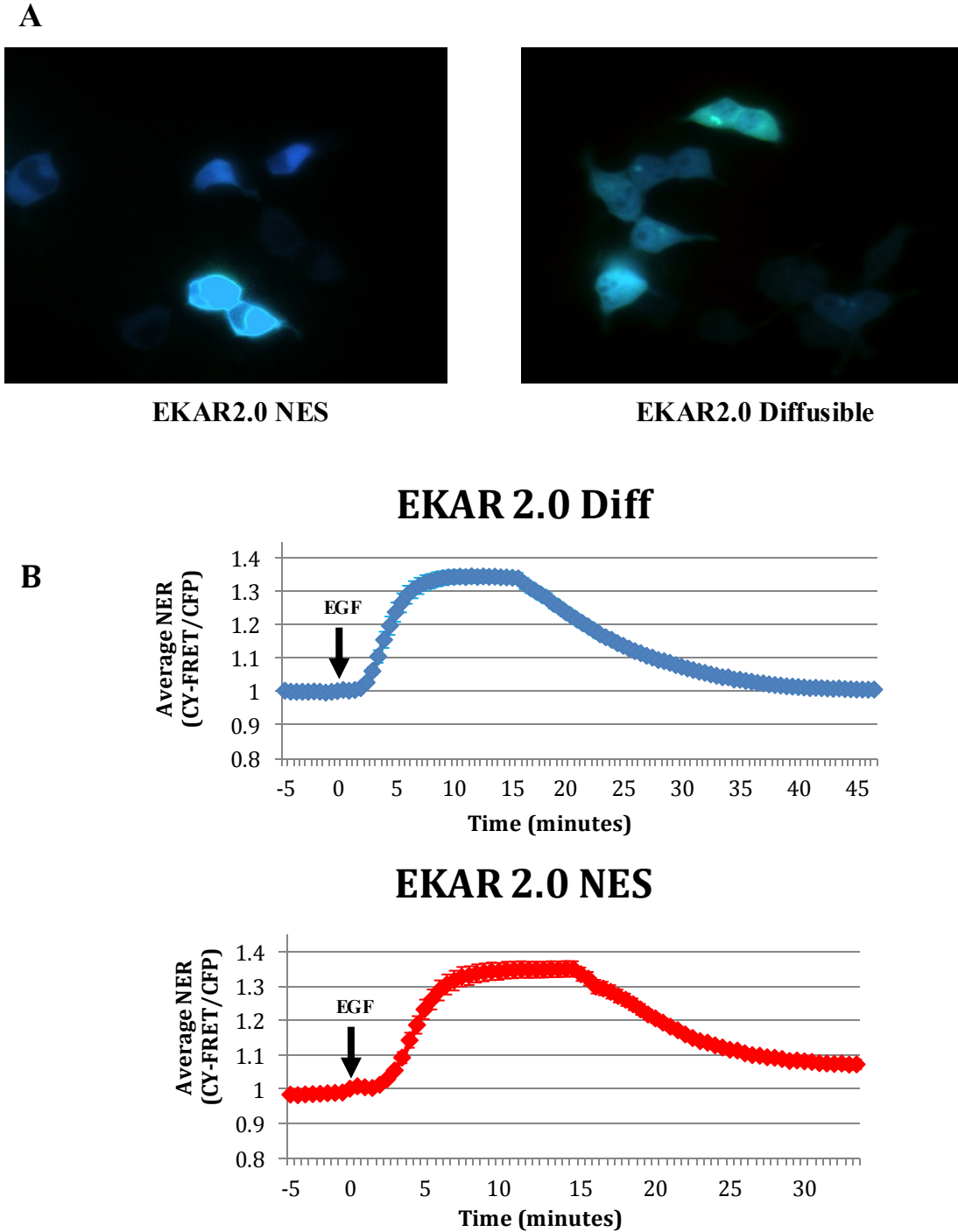


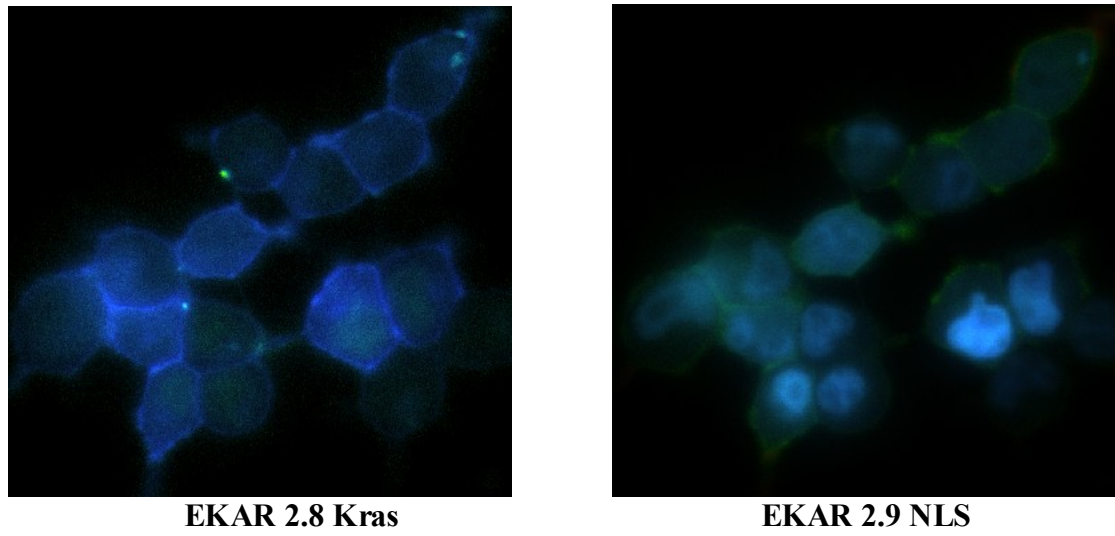
**Figure 2.4:** Cytoplasmic targeting of EKAR. A) Localization of NES-tagged EKAR to the cytoplasm and diffusible EKAR. B) Response comparison of NES-tagged and diffusible EKAR in HEK293 cells stimulated by 100ng/mL EGF.

### **ERK activity in the plasma membrane and nucleus**

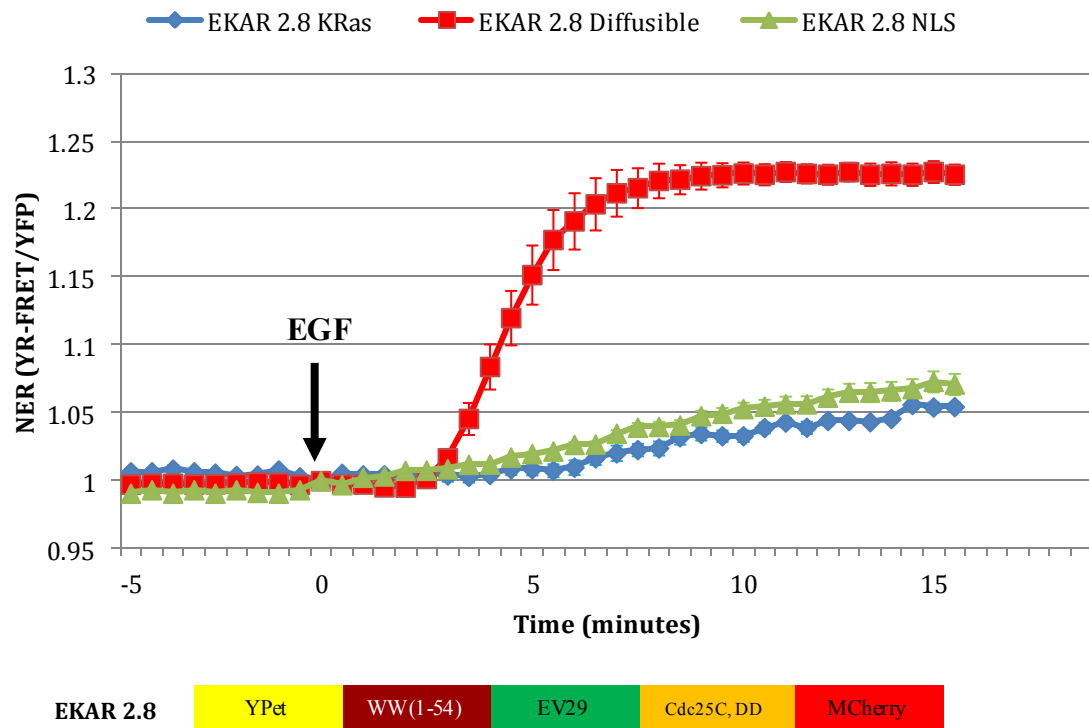
In resting cells, ERK and its upstream activators are primarily located in the cytoplasm. Upon stimulation, a great majority of active ERK rapidly detaches from cytoplasmic anchoring proteins and translocates to the nucleus, where it acts on target substrates (9). Two major mechanisms believed to control active ERK translocation to the nucleus include passive diffusion and active transport of ERK dimers (10). ERK activity in the nucleus is regulated through export from the nucleus and by dephosphorylation via MAP kinase phosphatases, which have induced expression downstream of the ERK pathway (11). The distribution of active ERK between the cytoplasm and nucleus, as well as the duration of active ERK in the nucleus are strong determinants for signal specificity (12). Alternatively, the roughly 25-35% of ERK molecules that do not detach remain in the cytoplasm via binding of anchoring proteins with high affinity for inactive ERK and MEK. Due to this close proximity with MEK, inactive ERK will likely be activated closer to upstream components of the pathway which are localized in the plasma membrane. Moreover, it has been suggested that such scaffolds may show a stimulus-dependent increase in scaffold protein affinity for inactive ERK (13). Such scaffolds can also tether other upstream components involved in ERK activation, including ERK, to the plasma membrane and facilitate ERK activation. After activation, ERK activity in the plasma membrane serves a role in the negative feedback of the pathway. Through direct phosphorylation of many targets including receptors (e.g. EGFR), nucleotide exchange factors (e.g. Sos), and upstream kinases (Raf and MEK), ERK acts to turn off this pathway.

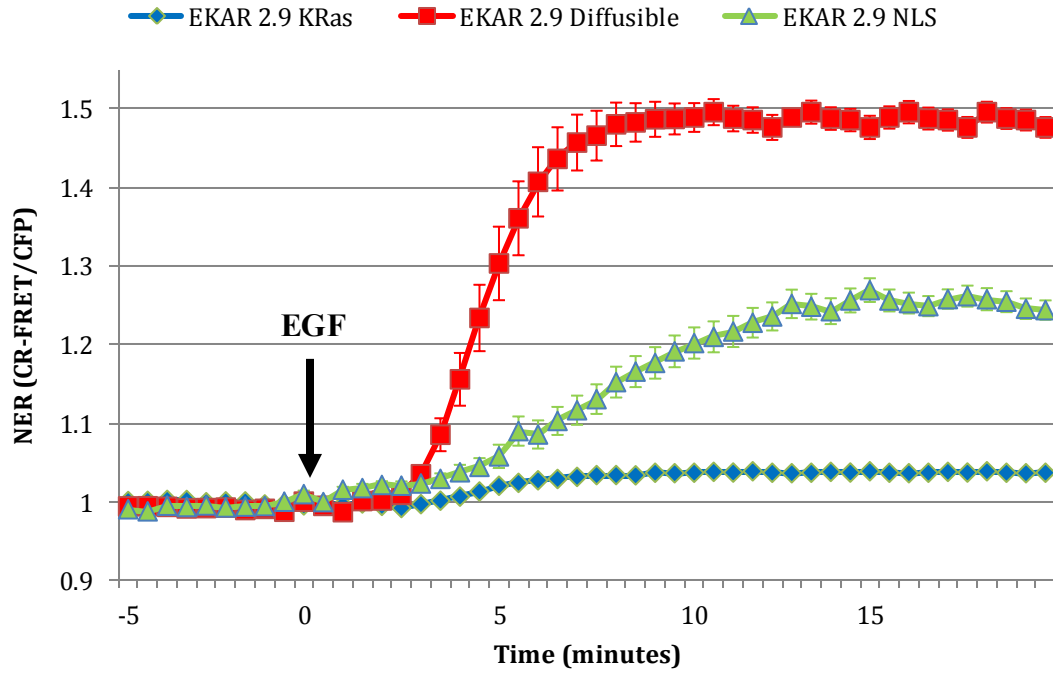
To further investigate ERK activity dynamics in the plasma membrane and nucleus, tagged versions of EKAR were developed with a C-terminal CAAX sequence from K-Ras and nuclear localization signal (NLS) sequence, respectively. As shown in Figure 2.5A, targeting of EKAR to the plasma membrane or nucleus provides strong and exclusive fluorescence in the respective compartments. Interestingly, the subcellular localization of EKAR in both the plasma membrane and nucleus did show reduced dynamic ranges and delays in the responses of the plasma membrane (Figure 2.5B). The reduced dynamic ranges and differences in response kinetics could be due to intrinsic aspects of a particular sensor in a certain environment or cross contamination of fluorescence in adjacent compartments. However, similar trends in amplitude and kinetic differences were observed for each of the similarly targeted EKAR color variants. Thus, it is concluded that the targeted versions of EKAR can provide accurate dynamic ERK activity information in different compartments.

**A**



**B**





EKAR 2.9    MCherry    WW(1-54)    EV29    Cdc25C, DD    ECFP

**Figure 2.5:** Plasma membrane and nuclear targeting of EKAR. A) Localization of KRas-tagged EKAR to the plasma membrane and NLS-tagged EKAR to the nucleus. B) Response comparison of tagged versions of Yellow-Red EKAR (top) and tagged versions of Cyan-Red EKAR (bottom) in HEK293 cells stimulated by 100ng/mL EGF.

## **Co-Imaging of subcellular targeted EKAR**

As previously described, one of the major mechanisms contributing to the specificity of ERK activation to a particular stimulus is the dynamic localization of different components of the ERK pathway (14, 15). At rest, ERK shows a primarily diffusive nature in the cytoplasm, typical of kinases (16). This nature of ERK is due to several strong interactions that it has with a number of anchoring proteins. Upon stimulation, the localization of components of the ERK cascade becomes dynamic. Raf1 is recruited to the plasma membrane, where it interacts with Ras. Activated MEK and ERK are released from cytoplasmic anchors, where they can act on their respective cytoplasmic targets or translocate to the nucleus. The multitude of cytoplasmic proteins, both anchoring proteins and downstream substrates, that interact with ERK greatly regulate ERK signaling specificity (17). With the differential expression of proteins across different cell types, the dynamics of ERK activity in different compartments are cell-specific.

As a tool to investigate the spatio-temporal dynamics of ERK activation, targeted versions of the EKAR color variants were utilized for co-imaging to dissect the dynamics at two different cellular compartments simultaneously. For this strategy, we combined distinctly targeted EKAR color variants of spectrally distinct donor FPs, ECFP and YPet, with a common acceptor FP, MCherry. This allows for distinct fluorescence-based resolution of ERK activity in different subcellular compartments. In a more physiological cell type, the MIN6 pancreatic beta cell line, we examine the EGF-induced dynamics of ERK activity in the plasma membrane, cytosolic, and nuclear compartments. While experimentation was done to visualize ERK activity dynamics in two compartments

simultaneously, representative results compiling ERK activity in each compartment are overlaid and shown in Figure 2.6.



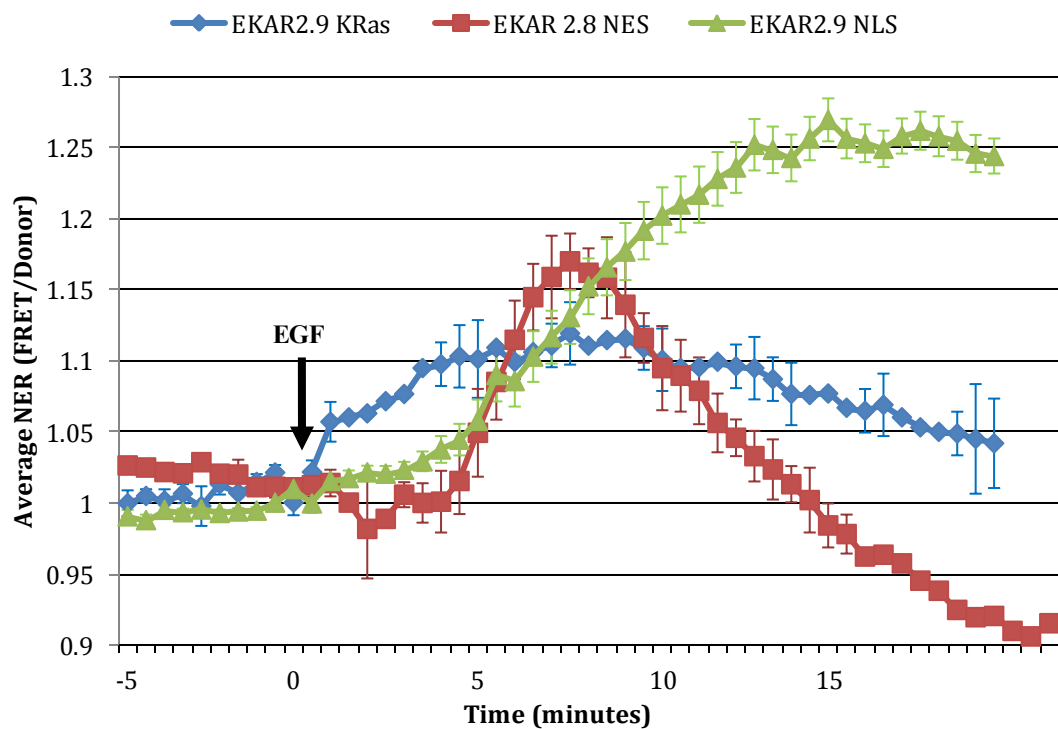


**Figure 2.6:** Targeted EKAR Co-Imaging. Compiled results showing ERK activity dynamics in the plasma membrane (blue), cytosol (red), and nucleus (green) in the MIN6 pancreatic beta cell line stimulated by 100ng/mL epidermal growth factor (EGF).

Our results show the progression of ERK activation from the plasma membrane to the nucleus. Upon EGF stimulation, ERK is rapidly activated with  $t_{1/2} = 2.68 \pm 0.49$  minutes and shows a sustained response that begins slowly decreasing after 10 minutes. In the cytoplasm, ERK shows a transient response with a  $t_{1/2} = 5.93 \pm 0.26$  minutes that begins decreasing at a similar rate as cytoplasmic ERK activation 8 minutes after EGF stimulation. The transient cytoplasmic response is consistent with the rapid shuttling of ERK to the nucleus as it is activated. This is also observed by comparing the slopes of linear regions of the cytoplasmic ERK activity decrease ( $m = -2.87 \text{ \%}/\text{min}$ ) and the nuclear ERK activity increase ( $m = 2.52 \text{ \%}/\text{min}$ ). Further studies with these tools would support investigations to elucidate the mechanisms involved in the translocation of activated ERK into the nucleus. Moreover, these tools can be used to elucidate spatio-temporal mechanisms contributing to the tight regulation of ERK activation and deactivation kinetics in different compartments.

## Methods

**Gene construction of EKARs.** Variants of cyan, red, and yellow fluorescent proteins [ECFP, Cerulean, Mcherry, and YPet] were PCR amplified with the appropriate restriction digest sites for incorporation into EKAR2.3 by replacing the ECFP or YPet fluorescent proteins. The series of EKAR constructs were generated in pRSET B (Invitrogen) and then subcloned to pcDNA3 (Invitrogen) for high-level, stable, and transient expression in mammalian cells.

**Cell culture and imaging.** HEK-293 cells were plated on sterilized glass coverslips in 35-mm dishes and grown to ~50% confluency in Dulbecco's modified eagle medium (DMEM) with 10% Fetal bovine serum (FBS) at 37°C and 5% CO<sub>2</sub>. Cells were transfected with Lipofectamine2000 and allowed to grow 20-24 hours before imaging. After washing twice with Hanks' balanced salt solution, cells were maintained in buffer for the duration of the experiments. MIN6 cells were plated on sterilized glass cover-slips in 35-mm dishes and grown to ~50% confluency in DMEM with 10% (FBS) and 5% Donor horse serum (DHS) at 37°C and 5% CO<sub>2</sub>. Cells were transfected with Lipofectamine2000 and grown for 40-50 hours before imaging. Epidermal growth factor (Human EGF) and U0126 (Sigma) were utilized as indicated.

Experiments were conducted on a Zeiss Axiovert 200M microscope with a 40x/1.3NA oil-immersion objective and cooled charge-coupled-device camera (MicroMAX BFT512; Roper Scientific, Trenton, NJ) controlled by METAFLUOR software (Molecular Devices, Sunnyvale, CA). Dual cyan-red emission ratio imaging required a 420DF20 excitation filter, 475DF40 and 653DF95 emission filters for CFP and RFP, respectively, and a 450DRLP dichroic mirror. Dual yellow-red emission ratio imaging required a 495DF10 excitation filter, 535DF25 and 653DF95 emission filters for YFP and RFP, respectively, and a 515DRLP dichroic mirror. Raw fluorescent images were reanalyzed and corrected using the METAFLUOR software and MATLAB (MathWorks Inc., Natick, MA) to subtract background fluorescent and for normalization by the basal emission ratios, such that the emission ratios before drug stimulation are set with a value of unity.

## References

1. Bourgeois, D. and Adam, V. (2012) *Life* 64, 482-491.
2. Day, R.N. and Davidson, M.W. (2009) *Chem. Soc. Rev.* 38, 2887-2921.
3. Ouyang, M., Sun, J., Chien, S., and Wang, Y. (2008) *Proc. Natl. Acad. Sci. U. S. A.* 105, 14353-14358.
4. Woehler, A. (2013) *PLoS One* 8, e61096.
5. Ai, H.W., Hazelwood, K.L., Davidson, M.W., Campbell, R.E. (2008) *Nat. Methods* 5, 401-403.
6. Shaner, N.C., Lin, M.Z., McKeown, M.R., Steinbach, P.A., Hazelwood, K.L., Davidson, M.W., Tsien, R.Y. (2008) *Nat. Methods* 5, 545-551.
7. Piljic, A., Schultz, C. (2008) *Chem. Biol.* 3, 156-160.
8. DiPilato, L.M., Cheng, X., and Zhang, J. (2004) *Proc. Natl. Acad. Sci. USA* 101, 16513-16518.
9. Zehorai, E., Yao, Z., Plotnikov, A., Seger, R. (2010) *Molec. Cell. Endocrinol.* 314, 213-220.
10. Casar, B., Pinto, A., Crespo, P. (2008) *Mol. Cell.* 31, 708-721.
11. Volmat, V., Camps, M., Arkinstall, S., Pouyssegur, Lenormand, P. (2001) *J. Cell. Sci.* 114, 3433-3443.
12. Xu, L., and Massague, J. (2004) *Nat. Rev. Mol. Cell. Biol.* 5, 209-219
13. Lee, T., Hoofnagle, A.N., Kabuyama, Y., Stroud, J., Min, X., Goldsmith, E.J., Chen, L., Resing, K.A., Ahn, N.G. (2004) *Mol. Cell.* 14, 43-55
14. Mor, A., Philips, M.R. (2006) *Annu. Rev. Immunol.* 24, 771-800.
15. Hekman, M., Hamm, H., Villar, A.V., Bader, B., Kuhlman, J., Nickel, J., Rapp, U.R. (2002) *J. Biol. Chem.* 277, 24090-24102.

16. Chuderland, D., Seger, R. (2005) *Mol. Biotechnol.* 29, 57-74.
17. Shaul, Y.D., Seger, R. (2007) *Biochim. Biosphys. Acta* 1773, 1213-1226.

## **Chapter 3**

### **Investigation of Crosstalk and Pathway dynamics of Extracellular Signal-Regulated Kinase**

### **Biological crosstalk: cAMP-PKA and ERK-MAPK pathways**

Cells are constantly exposed to a number of different biochemical and biophysical cues which activate signaling pathways. How a cell makes a specific response to an environmental cue is determined by tight regulations on the signaling intensity and duration of several pathways. Kinases are key players in biological crosstalk, in which components of one pathway can affect another, due to the sheer number of downstream targets. A notable example of the role signaling crosstalk can have in controlling cellular responses occurs from interactions between components of the cAMP-PKA and ERK-MAPK pathways to regulate cellular proliferation (1). In many cell types, cAMP has been shown to inhibit or delay cellular proliferation signals (2-4). cAMP has been proposed to inhibit ERK activity through its upstream MAPKKK, Raf. A number of mechanisms have been proposed whereby the cAMP-dependent kinase, Protein kinase A (PKA) either indirectly causes the sequestration of C-RAF or directly phosphorylates C-RAF and block its activation by Ras. While the cAMP-PKA pathway and ERK-MAPK pathways are primarily activated through different receptors and the cAMP-PKA pathway acts to inhibit ERK signaling, crosstalk between the two is not one-sided. Of the many ERK targets, phosphodiesterase PDE4 acts to convert cAMP into AMP. Phosphorylation of long PDE4 isoforms by ERK inactivates the enzyme and causes an increase in cAMP levels, representing a negative feedback mechanism of ERK signaling. On the other hand, phosphorylation of short PDE4 isoforms activates the enzyme and prevents cAMP-dependent inactivation of ERK signaling (5). The complex coupling of both positive and negative connections between the two pathways is inherently important for cells to appropriately transduce signals. To visualize the complex dynamics of the two

pathways, it would be ideal to correlate PKA and ERK activity simultaneously. To address this objective, the previously described EKAR color variants will be used with color variants of a PKA activity reporter, AKAR.

### **EKAR and AKAR co-imaging.**

Given the complex nature of biological crosstalk, the simultaneous utilization of multiple FRET-based kinase activity reporters on a single cell level would enhance analyses. For this task, biosensors must be engineered with fluorescent proteins with smaller degrees of spectral overlap, compared to Cyan-Yellow, to allow for the use of multiple sensors, minimize fluorescent cross contamination, and yet still allow strong FRET signals to allow for visualization. Using the developed and characterized color variants of EKAR with previously developed color variants of AKAR (6), we examine the capability of visualizing PKA and ERK activities simultaneously.

To examine both the activation and deactivation of ERK and PKA activity, we utilized the following:

1. Epidermal growth factor (EGF) 100ng/mL to stimulate the ERK-MAPK pathway
2. Forskolin (FsK) 50 $\mu$ M, which activates adenylate cyclase and thus increasing cAMP levels, to activate PKA
3. 3-isobutyl-1-methylxanthine (IBMX) 100 $\mu$ M, a competitive and non-selective phosphodiesterase inhibitor, to maximize PKA activation
4. 1,4-diamino-2,3-dicyano-1,4-bis[2-aminophenylthio] butadiene (U0126) 20 $\mu$ M, a selective MEK1 and MEK2 inhibitor



#### 5. N-[2-bromocinnamylamino) ethyl]-5-isoquinoline sulfonamide (H89)

20 $\mu$ M, a competitive inhibitor of the ATP site on the PKA catalytic subunit.

Co-imaging experiments were conducted utilizing Yellow-Red and Cyan-Red color combinations of the two probes in HEK293 cells. Upon EGF stimulation, we observed the previously observed kinetics for EKAR2.9; however, with a diminished dynamic range of about 50%, compared to sole-imaging of the diffusible probe (Figure 3.1). Interestingly, we were able to visualize a minor increase in EGF-induced PKA activity, supporting evidence for the activation of PKA by the ERK-MAPK pathway. Upon a combined stimulation of Fsk and IBMX to maximize PKA activation, we observed similarly fast activation kinetics to previous results obtained from the AKAR color variant. Moreover, a corresponding 5% decrease of ERK activity is seen by Fsk and IBMX stimulation. A key observation is that maximal PKA activity does not completely deactivate ERK. As seen by the stimulation of the MEK inhibitor, U0126, ERK activity decreases further to near basal levels. Lastly, to confirm the reversibility of the AKAR reporter, we observe that H-89 stimulation does indeed inhibit PKA with similar deactivation kinetics to the previously published results (6). While the kinetics of each probe show comparable values under co-imaging to values obtained during sole-imaging, it is believed that the probes are still selectively reporting the activities of their respective kinases. However, the significant decreases of the dynamic ranges of both probes under co-imaging conditions, warrants investigation on the possibility of interactions between the probes. Experimental controls should elucidate whether the diminished dynamic ranges are due to intrinsic properties of the probes.

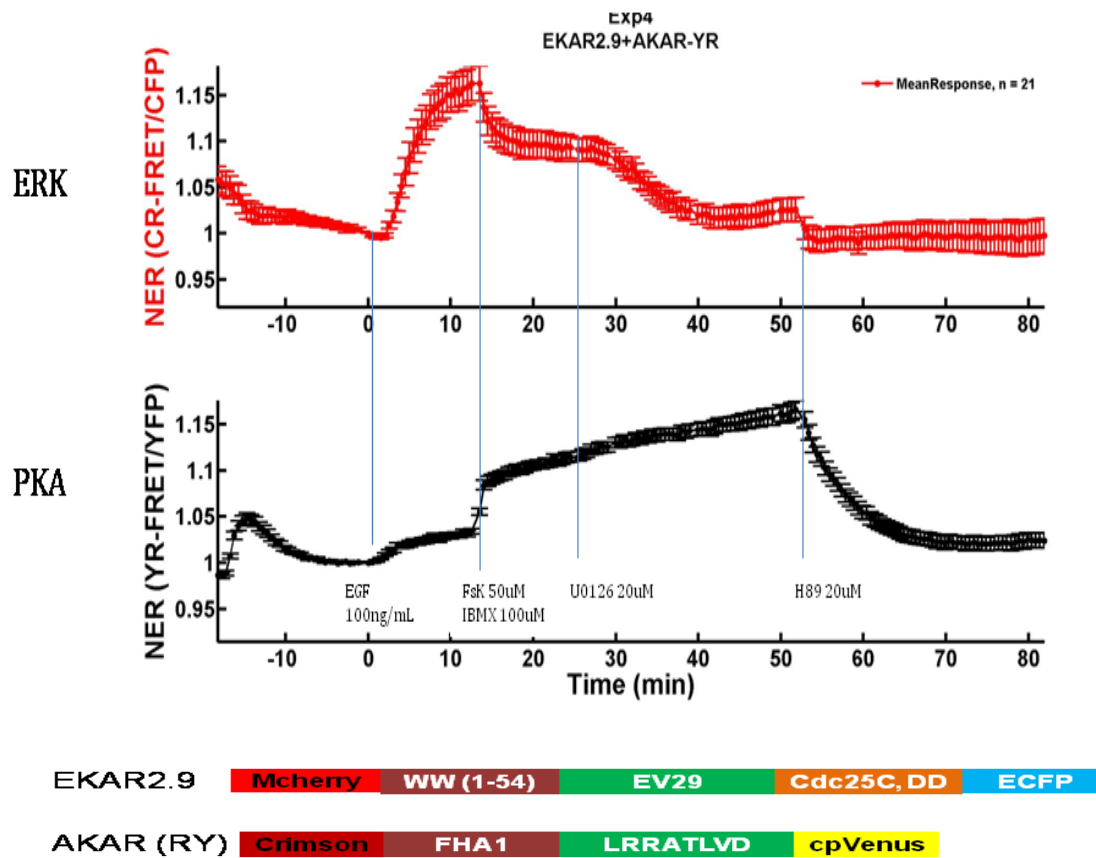


**Figure 3.1:** EKAR and AKAR co-imaging. Representative co-imaging results shown for Cyan-Red EKAR and Yellow-Red AKAR in HEK293 cells stimulated by 100ng/mL (EGF), 50 $\mu$ M Forskolin (FsK) + 100 $\mu$ M IBMX, 20 $\mu$ M U0126, and 20 $\mu$ M H89.

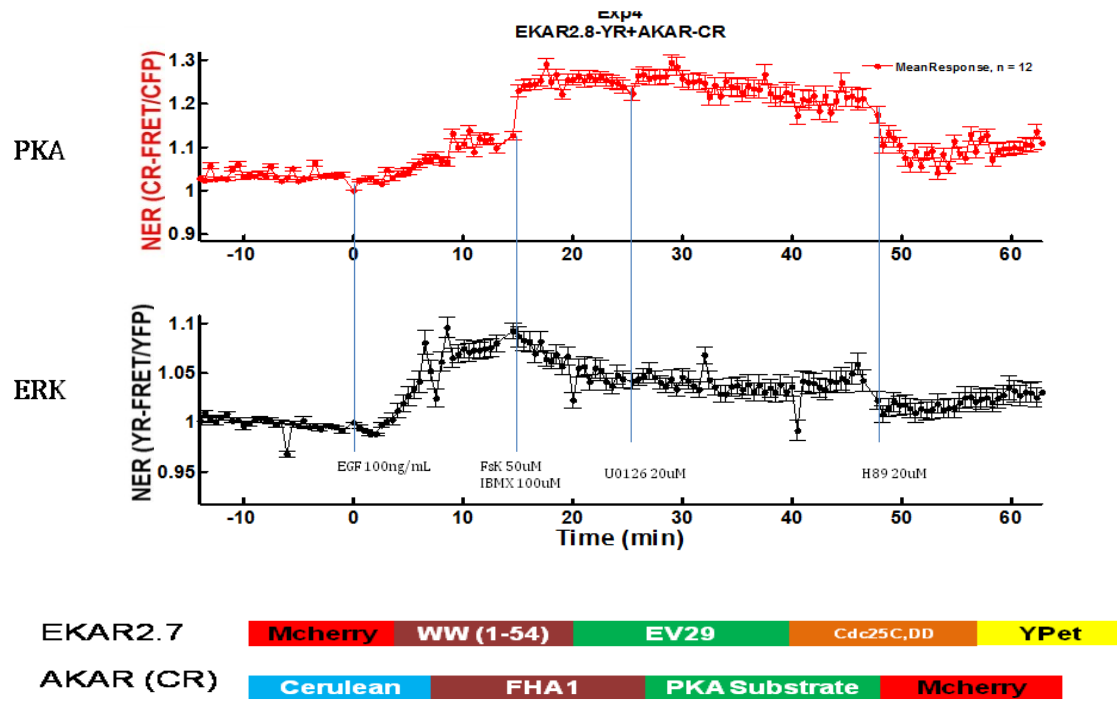
As a set of controls, we utilized non-phosphorylatable mutant (Thr-> Ala) versions of both the EKAR and AKAR probes to examine the potential of interference between the two probes, for example through interactions between the domains of different sensors or interference at the optical readout level. Co-imaging experiments conducted using Cyan-Red AKAR with wild-type (Figure 3.2A) or mutant versions (Figure 3.2B) of Yellow-Red EKAR showed similar amplitude and kinetics in the AKAR signal. Similar results were also seen for EKAR when co-imaged with wild-type and mutant AKAR. Moreover, the results show that the different FRET signals are still uniquely reporting on the activity of the respective kinases.

As another set of controls, we imaged the EKAR color variants alone under the same stimuli applications to examine the diminished dynamic range that are observed for both EKAR and AKAR during co-imaging. Under co-imaging conditions, Cyan-Red EKAR showed a roughly 70% decrease in EGF-response maximum amplitude compared to its sole-imaging response amplitude of  $45.9 \pm 4.8\%$  (Figure 3.3). Similarly, Yellow-Red AKAR, showed a roughly 50% decrease in the Fsk-induced maximum amplitude compared to the maximum amplitude under sole-imaging (6). Thus, we conclude that the two sensors are likely not interacting such that the specific readouts are perturbed.

Thus, while the temporal information of ERK and PKA activation and deactivation seem to be preserved, the dynamic range of the FRET-based sensors is diminished under EKAR and AKAR multiplexing with two distinct donor FPs and a common acceptor FP. Testing other FP variants or utilizing other strategies for multiplexing the two biosensors could provide additional means to examine ERK and PKA activity simultaneously with dynamic ranges comparable to those obtained when

solely utilizing one activity reporter. Fulfilling this objective would greatly enhance the capability to detect small amplitude changes in kinase activity.

A



**B**

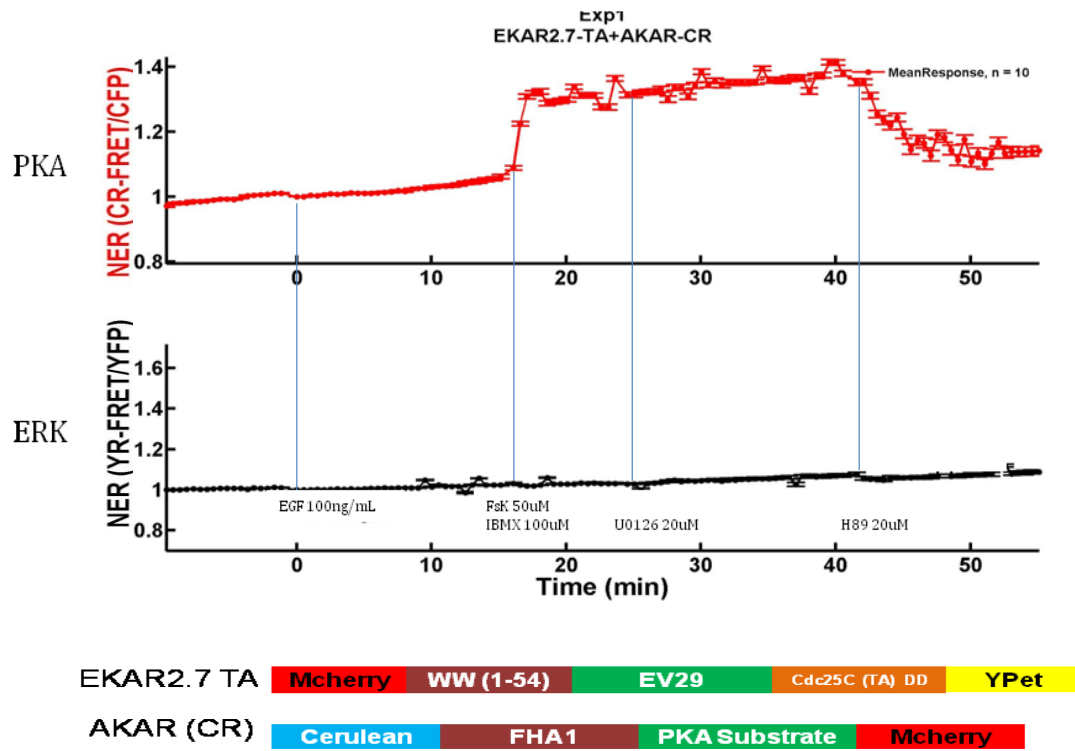


**Figure 3.2:** EKAR and AKAR co-imaging controls. Representative co-imaging results shown for Cyan-Red AKAR and Yellow-Red EKAR in HEK293 cells stimulated by 100ng/mL (EGF), 50 $\mu$ M Forskolin (FsK) + 100 $\mu$ M IBMX, 20 $\mu$ M U0126, and 20 $\mu$ M H89. A) Wild-type co-imaging of EKAR and AKAR. B) Kinase-dead EKAR mutant and wild-type AKAR co-imaging.

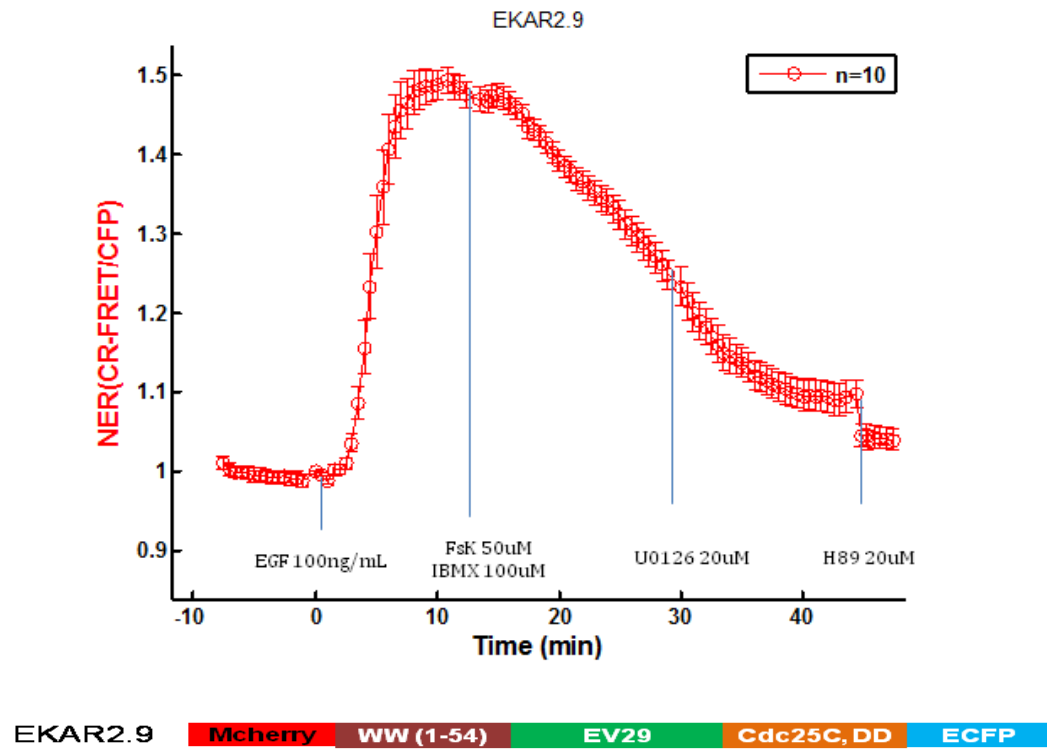


**Figure 3.3:** EK AR control under co-imaging stimulus conditions. Representative results for Cyan-Red AKAR EKAR in HEK293 cells stimulated by 100ng/mL (EGF), 50μM Forskolin (FsK) and 100μM IBMX, 20μM U0126, and 20μM H89.

=

### **Role of calcium in the ERK-MAPK pathway**

A number of signaling pathways are linked to second-messengers. Several examples of signaling pathways, including the ERK-MAPK and cAMP-PKA pathways, occurring through receptor tyrosine kinases (RTKs) and G-protein-coupled receptors have been shown to be linked the generation of inositol triphosphate and diacylglycerol through phospholipase C and the subsequent release of  $\text{Ca}^{2+}$  from intercellular stores. While calcium is known to have a role in several different cellular processes, a number of outstanding questions remain as to how exactly this divalent cation regulates the great diversity seen in cellular physiology. In the context of signaling pathways, these questions can be answered by elucidating how calcium is decoded through calcium sensing components in the pathways.

Calcium signals have been demonstrated in a number of signaling examples to carry information through their amplitude, spatial, and temporal characteristics (7-11). It has long been known that protein kinase C and calmodulin-dependent protein kinase II can unravel information contained in calcium signals (12). More recently, Ras has been shown to be a key node for decoding calcium signals through calcium-dependent Ras-activating guanine nucleotide exchange factors and Ras-deactivating GTPase-activating proteins (8). While the release of intracellular calcium is capable of activating many pathways, including activation of Ras signaling and the ERK-MAPK pathway, its role has been thought to be more strongly suited for determining signaling specificity rather than playing a vital role in Ras activation (9). While the FRET-based Ras activity reporters have aided investigations to on the important role that calcium plays in the



ERK-MAPK pathway, including key evidence that the activation of Raf1, downstream of Ras, occurs in a calcium-dependent manner (13), furthering the development of optical tools can help further elucidate the role of calcium on Ras activation and its effects on further downstream components of the ERK-MAPK pathway.

### **Simultaneously monitoring the activities of Ras and ERK**

To further expand the application of the developed EKAR color variants to further address questions on the role of calcium signals, we were inspired by a previously developed single-chain biosensor, ICUEPID, which is capable of simultaneously reporting PKA activity and cAMP dynamics (10). Interested to explore the dynamics of the ERK-MAPK pathway, it was ideal to develop a single sensor capable of providing orthogonal readouts on the activity of multiple components of this pathway simultaneously.

Utilizing a similar strategy by employing two donor FPs with distinct excitation and emission spectra (ECFP and YPet) sandwiching a common FRET acceptor FP (MCherry), a novel biosensor was developed to simultaneously report the activities of ERK and Ras, a membrane bound small GTPase, which activates the MAPKKK of the ERK-MAPK pathway, Raf. By combining the developed Yellow-Red EKAR with a previously developed and optimized Raichu-Ras-EV probe (14), the SABER (Simultaneous Activity Biosensor of ERK and Ras) was developed to investigate these activities in the plasma membrane compartment.

SABER was utilized to study calcium-induced activation of the ERK-MAPK pathway in MIN6 cells stimulated by tetraethylammonium chloride (TEA), a

pharmacological inhibitor of  $K^+$  channels that induces membrane polarization and robust  $Ca^{2+}$  oscillations (11, 15). As shown in Figure 3.4, SABER is capable of detecting the time delay between Ras and ERK activation with comparable kinetics to the Raichu-Ras-EV and EKAR-EV probes alone [Ras  $t_{1/2}$  = 1.14 +/- 0.1 min (mean +/- SEM) and ERK  $t_{1/2}$  = 4.55 +/- 1.16 min].

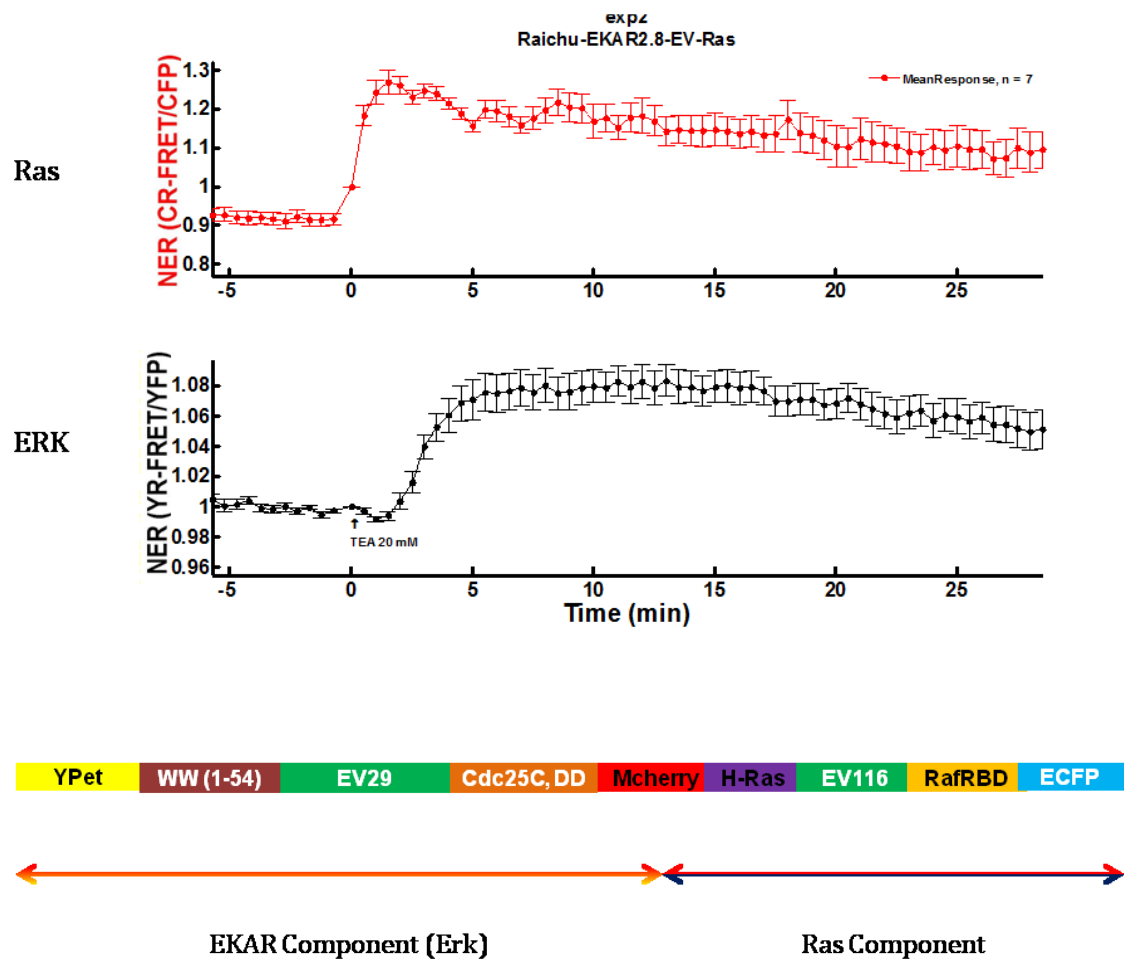


**Figure 3.4:** SABER1.0. Top) Representative mean results for SABER1.0 in MIN6 cells stimulated by 20mM TEA. Bottom) Domain Structure of SABER1.0

While the preservation of the kinetics of each sensor component is ideally met by SABER, the dynamic range, the maximum observed response, of the probe must be assessed to ensure the capability of detecting transient and small amplitude biochemical events. While not as easily apparent in the mean-value results, analysis of single cell data shows comparable amplitude responses for the EKAR component of SABER (Figures 3.5-3.6) in relation to the respective sole-imaging of Yellow-Red EKAR-EV ( $15.5 \pm 3.7$  %,  $n=37$ ). Moreover, the Ras activity reporter component of SABER shows a strong, yet slightly smaller amplitude response compared to the optimized Cyan-Yellow Raichu-Ras-EV ( $84.2 \pm 7.8$  %,  $n=4$ ).

Single cell response analyses reveal a great variety of Ras-responses, likely due to the differences in TEA-induced calcium responses among the cells. Interestingly, compared to the TEA-induced sustained Ras-responses (Figure 3.6), which have relatively slow ERK activation kinetics, TEA-induced Ras activity oscillations (Figure 3.5) have fast ERK activation kinetics, comparable to those observed for EGF-induced ERK activation.

Lastly, mutant versions of SABER are examined to ensure that preservation of the specificity of the Cyan-Red and Yellow-Red FRET signals for Ras and ERK activity, respectively (Figure 3.7). The mutation (Thr->Ala) in the ERK substrate domain of SABER, Cdc25C, abolishes the YR-FRET signal and reveals that the EKAR component of SABER is selective for monitoring ERK activity (Figure 3.7). A further study of SABER with a mutation in the Ras effector domain to reduce or abolish the affinity of Ras for guanine nucleotides should show a greatly diminished or abolished CR-FRET

signal. Such a result would show that the CR-FRET signal is selective for reporting Ras activity.

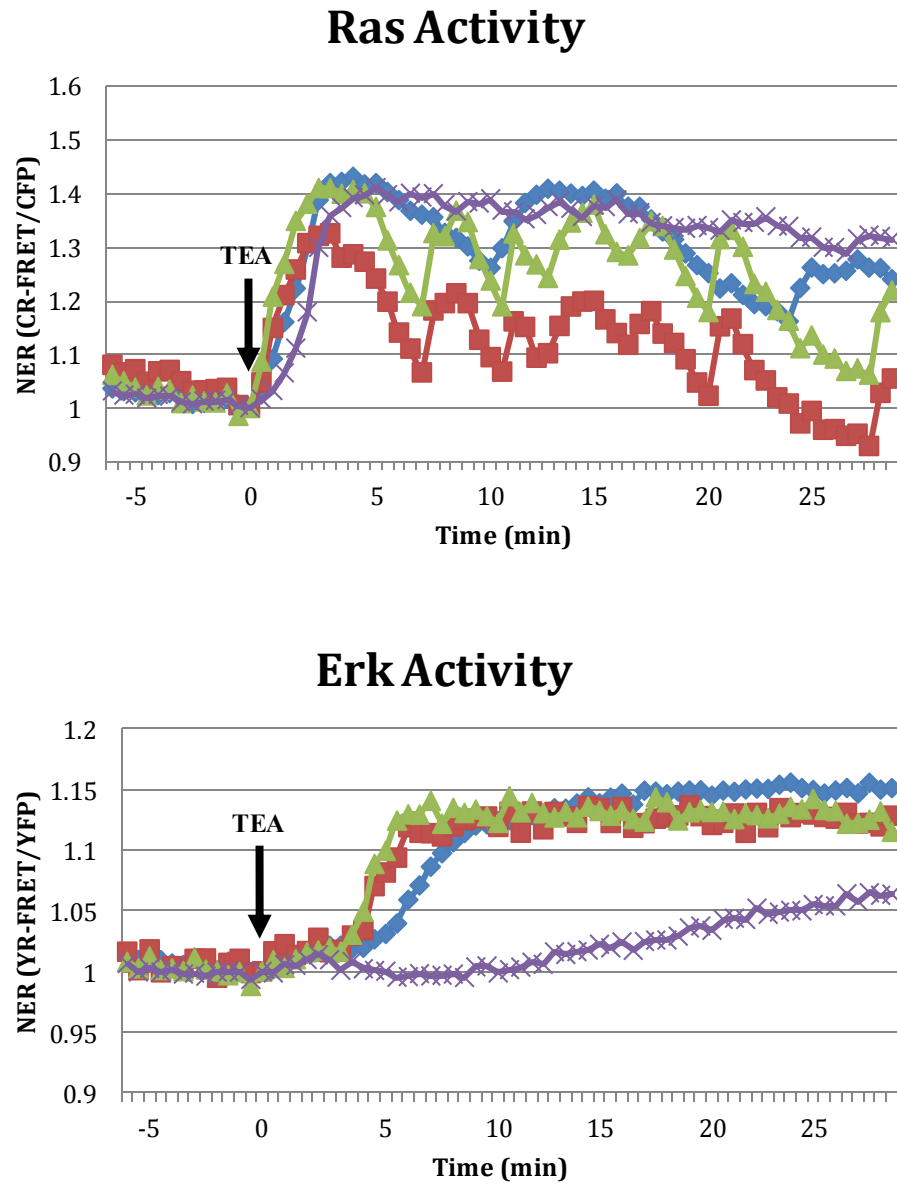


**Figure 3.5:** SABER1.0 single cell results - Oscillatory Ras Response. Representative results for oscillatory Ras responses in MIN6 cells stimulated by 20mM TEA. Ras and ERK activity responses from a cell are shown in the same color.

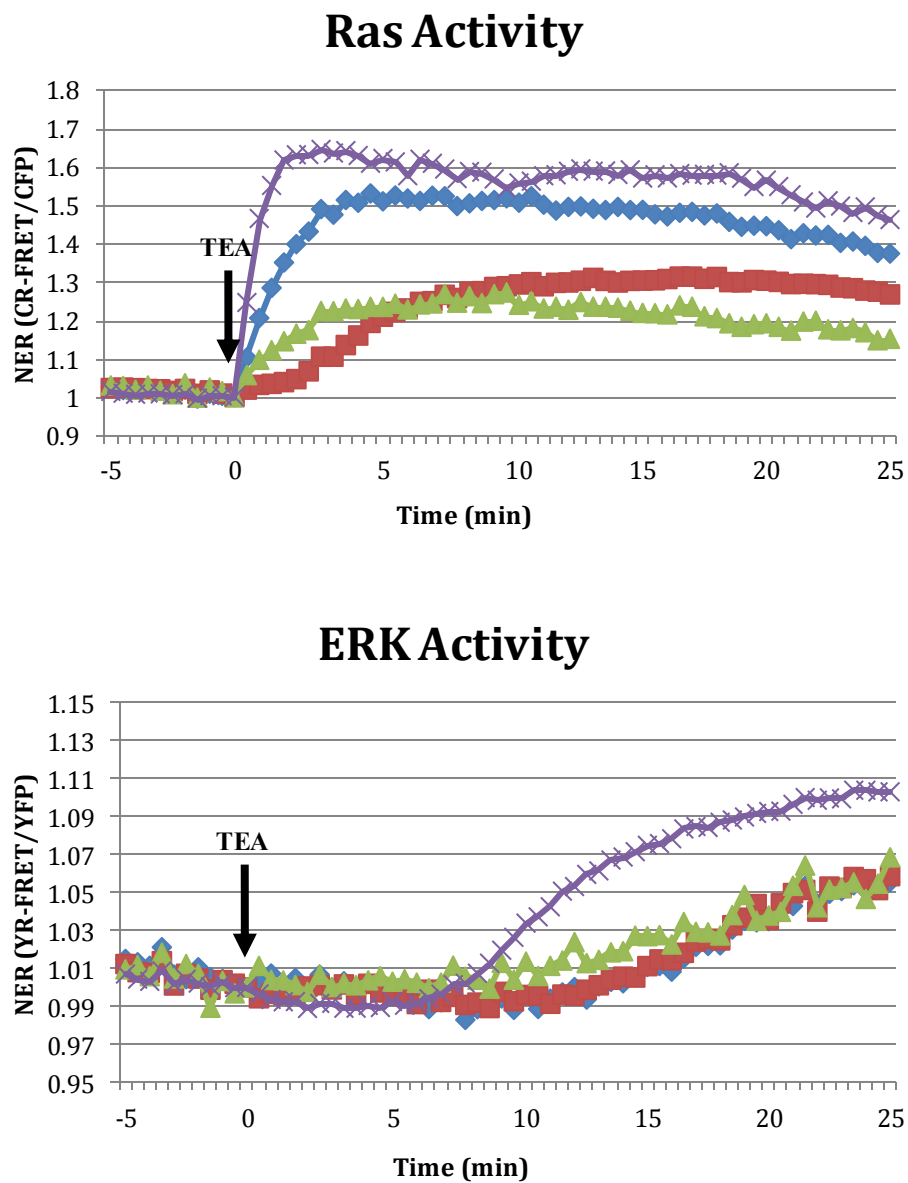


**Figure 3.6:** SABER1.0 single cell results - Sustained Ras Response. Representative results for sustained Ras responses in MIN6 cells stimulated by 20mM TEA. Ras and ERK activity responses from a cell are shown in the same color.

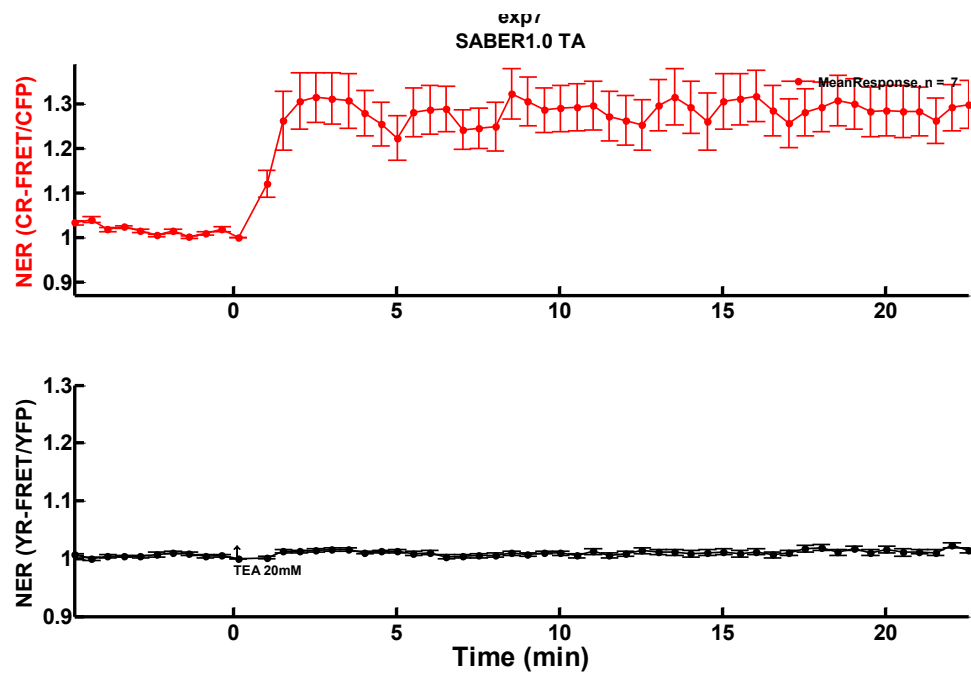


**Figure 3.7:** SABER1.0 mutant control. Mean-value results for SABER1.0 with a Thr → Ala mutation in the ERK substrate of EKAR, Cdc25C, in MIN6 cells stimulated by 20mM TEA.

The developed FRET-based EKAR color variants provide a means to simultaneously monitor the activity of ERK and the activity of another signaling component in live cells in a real-time manner. For two pathways that have been shown to decode calcium signals, the EKAR color variants serve as a tool in conjunction with previously developed AKAR variants to correlate ERK and PKA activities simultaneously. Our results confirm biological responses and feedback mechanisms of ERK and PKA activity as seen by their responses to activators and inhibitors of each kinase. Yet, the precise correlation of both activities simultaneously provided by the use of the color variant strategy provides the field of biological signaling a powerful tool to further understand ERK-PKA pathway crosstalk.

The combination of the EKAR-EV and Raichu-Ras-EV probes into the single-chain SABER biosensor, utilizing a similar FRET-pair strategy as ICUEPID, provides a novel biosensor capable of simultaneously monitoring both ERK and Ras activities in the plasma membrane. With the temporal and max amplitude characteristics of each component generally conserved, SABER allows for correlating ERK and Ras activity dynamics with strong precision on a single-cell basis. Furthermore, if used in conjunction with a calcium level indicator, investigations on the role of calcium in regulating Ras activity and the downstream ERK-MAPK pathway dynamics can provide crucial knowledge on how signaling diversity is controlled by coded information in calcium signals.



## Methods

**Gene construction of SABER.** Yellow-Red EKAR-EV and Cyan-Yellow Raichu-Ras-EV were PCR amplified with the appropriate restriction digest sites for incorporation of the Yellow-Red EKAR-EV into the Raichu-Ras-EV probe by replacing its N-terminal YPet fluorescent protein. The SABER DNA construct was generated in pRaichu plasmid backbone for high-level, stable, and transient expression in mammalian cells.

**Cell culture and imaging.** HEK-293 cells were plated on sterilized glass coverslips in 35-mm dishes and grown to ~50% confluency in Dulbecco's modified eagle medium (DMEM) with 10% Fetal bovine serum (FBS) at 37°C and 5% CO<sub>2</sub>. Cells were transfected with Lipofectamine2000 and allowed to grow 20-24 hours before imaging. After washing twice with Hanks' balanced salt solution, cells were maintained in buffer for the duration of the experiments. MIN6 cells were plated on sterilized glass coverslips in 35-mm dishes and grown to ~50% confluency in DMEM with 10% (FBS) and 5% Donor horse serum (DHS) at 37°C and 5% CO<sub>2</sub>. Cells were transfected with Lipofectamine2000 and grown for 40-50 hours before imaging. Epidermal growth factor (Human EGF), FsK (Calbiochem), IBMX (Sigma), U0126 (Sigma), H89 (Sigma), and TEA (Sigma) were utilized as indicated.

Experiments were conducted on a Zeiss Axiovert 200M microscope with a 40x/1.3NA oil-immersion objective and cooled charge-coupled-device camera (MicroMAX BFT512; Roper Scientific, Trenton, NJ) controlled by METAFLUOR software (Molecular Devices, Sunnyvale, CA). Dual cyan-red emission ratio imaging required a 420DF20 excitation filter, 475DF40 and 653DF95 emission filters for CFP and

RFP, respectively, and a 450DRLP dichroic mirror. Dual yellow-red emission ratio imaging required a 495DF10 excitation filter, 535DF25 and 653DF95 emission filters for YFP and RFP, respectively, and a 515DRLP dichroic mirror. Raw fluorescent images were reanalyzed and corrected using the METAFLUOR software and MATLAB (MathWorks Inc., Natick, MA) to subtract background fluorescent and for normalization by the basal emission ratios, such that the emission ratios before drug stimulation are set with a value of unity.

## References

1. Dumaz, N., Marais, R. (2005) *FEBS J.* 272, 3491-3504.
2. Schmitt, J.M. and Stork, P.J. (2002) *Mol. Cell. Biol.* 21, 3671-3683.
3. Almela, P., Atucha, N.M., Milanes, M.V., Laorden, M.L. (2009) *JPET* 330: 771-782.
4. Stork, P.J. (2003) *Trends Biochem. Sci.* 28, 267-275.
5. Baillie, G.S., MacKenzie, S.J., McPhee, I., Houslay, M.D. (2000) *EMBO J.* 18, 893-903.
6. Aye-Han, N.N., Allen, M.D., Ni, Q., Zhang, J. (2012) *Mol. Biosyst.* 8, 1435-1440.
7. Dolmettsch, R.E., Xu, K., Lewis, R.S. (1998) *Nature* 392, 933-936.
8. Walker, S.A., Lockyer, P.J., Cullen, P.J. (2003) *Biochem. Soc. Trans.* 31, 966-969.
9. Kupzig, S., Walker, S.A., Cullen, P.J. (2005) *Proc. Natl. Acad. Sci. U.S.A.* 102, 7577-7582.
10. Ni, Q., Ganesan, A., Aye-Han, N.N., Gao, X., Allen, M.D., Levchenko, A., Zhang, J. (2011) *Nat. Chem. Biol.* 7, 34-40.
11. Mehta, S., Aye-Han, N.N., Ganesan, A., Oldach, L., Gorshkov, K., Zhang, J. (2014) *eLife* 3, e03765.
12. DeKoninck, P. and Schulman, H. (1998) *Science* 279, 227-230.
13. Yoshiki, S., Matsunaga-Udagawa, R., Aoki, K., Kamioka, Y., Kiyokawa, E., Matsuda, M. (2010) *Mol. Biol. Cell* 21, 1088-1096.
14. Komatsu, N., Aoki, Y., Yamada, M., Yukinaga, H., Fujita, Y., Kamioka, Y., Matsuda, M. (2011) *Mol Biol Cell* 22, 4647-4656.
15. Landa, L.R., Harbeck, M., Kaihara, K., Chepurny, O., Kitiphongspattana, K., Graf, O., Nikolaev, V. O., Lohse, M.J., Holz, G.G., Roe, M.W. (2005) *J. Biol. Chem.* 280, 31294-31302.

**Archer R. Hamidzadeh**

E-mail: [Ahamidz1@jhu.edu](mailto:Ahamidz1@jhu.edu);

Cell: (615) 403-9904

Country of Citizenship: USA

**Permanent Address**

501 Dekemont Lane  
Apt 824  
Brentwood, TN 37027  
21205

**Current Address**

929 N. Wolfe Street  
  
Baltimore, MD

---

**EDUCATION**

M.S.E. Biomedical Engineering; Johns Hopkins University, Baltimore, MD; *September 2013 – Present*

Thesis Project: *Optical FRET-Based Tools to Elucidate Extracellular Signal-Regulate Kinase (ERK) Dynamics*

**Advisors** : Dr. Jin Zhang, Professor of Pharmacology and Molecular Sciences, Johns Hopkins University

Dr. Andre Levchenko, John C. Malone Professor of Biomedical Engineering, Yale University

B.S. Bachelor of Science in Biomedical Engineering; Johns Hopkins University, Baltimore, MD; *September 2010 – May 2013*

Bachelor of Science in Cellular and Molecular Biology; Johns Hopkins University, Baltimore, MD; *September 2010 – May 2013*

**RESEARCH EXPERIENCE**

- Graduate Research Assistant in the Department of Biomedical Engineering, Johns Hopkins University; *September 2013 – Present*; **Advisors** : Dr. Jin Zhang and Dr. Andre Levchenko
- Undergraduate Research Assistant in the Department of Biomedical Engineering, Signal Transduction and Cell-Cell Communication Lab, Johns Hopkins University; *September 2011 – July 2013*; **Advisor**: Dr. Andre Levchenko
- Summer Research Internship at Vanderbilt University in the Vanderbilt Summer Diabetes Research Program; *May 2011 – August 2011*; **Advisors** : Dr. John Wikswo and Dr. Richard O'Brien
- Undergraduate Research Assistant in the Department of Biology at Johns Hopkins University; *December 2010 – May 2012*; **Advisor**: Professor Vincent J. Hilser